Transcriptional repression of oestrogen receptor by metastasis-associated protein 1 corepressor

Abhijit Mazumdar*†, Rui-An Wang*†, Sandip K. Mishra*, Liana Adam*, Rozita Bagheri-Yarmand*, Mahitosh Mandal*, Ratna K. Vadlamudi* and Rakesh Kumar*‡

**Department of Molecular and Cellular Oncology, University of Texas M. D. Anderson Cancer Center, 1515 Holcombe Boulevard, Houston, Texas 77030, USA*
†These authors contributed equally to this work
‡e-mail: rkumar@notes.mdacc.tmc.edu

Activation of the heregulin/HER2 pathway in oestrogen receptor (ER)-positive breast-cancer cells leads to suppression of oestrogen-receptor element (ERE)-driven transcription and disruption of oestradiol responsiveness, and thus contributes to progression of tumours to more invasive phenotypes. Here we report the identification of metastatic-associated protein 1 (MTA1), a component of histone deacetylase (HDAC) and nucleosome-remodelling complexes, as a gene product induced by heregulin-β1 (HRG). Stimulation of cells with HRG is accompanied by suppression of histone acetylation and enhancement of deacetylase activity. MTA1 is also a potent corepressor of ERE transcription, as it blocks the ability of oestradiol to stimulate ER-mediated transcription. The histone-deacetylase inhibitor trichostatin A blocks MTA1-mediated repression of ERE transcription. Furthermore, MTA1 directly interacts with histone deacetylase-1 and -2 and with the activation domain of ER-α. Overexpression of MTA1 in breast-cancer cells is accompanied by enhancement of the ability of cells to invade and to grow in an anchorage-independent manner. HRG also promotes interaction of MTA1 with endogenous ER and association of MTA1 or HDAC with ERE-responsive target-gene promoters *in vivo*. These results identify ER-mediated transcription as a nuclear target of MTA1 and indicate that HDAC complexes associated with the MTA1 corepressor may mediate ER transcriptional repression by HRG.

Growth of human breast cells is closely regulated by receptors of both steroid and peptide hormones[1]. Members of both receptor classes are important prognostic factors in human breast cancer as well as determinants of endocrine therapy in breast cancer patients. After the initial stages of breast-cancer progression, tumours frequently acquire resistance to -steroid hormones with concurrent amplification of growth-factor receptors; this alteration is associated with a poor prognosis. For example, overexpression of c-*erb*B-2 (also known as human epidermal growth-factor receptor, HER2) in ER-positive breast-cancer cells leads to reduced sensitivity of these cells to oestrogen both *in vitro* and *in vivo*[2–5]. In addition, accumulating evidence indicates that the progression of breast-cancer cells to a more invasive phenotype may be regulated not only by HER2 overexpression but also by a mesenchymal growth factor, HRG, which is a ligand for HER3 and HER4 and which transactivates HER2 (ref. 6). Recently, we and others have shown that HRG activation promotes the development of aggressive phenotypes in breast-cancer cells[7–10].

There is also considerable evidence to indicate that the development of hormone independence in breast cancer cells may be influenced by crosstalk between steroid-hormone and HER2/HRG pathways. For example, expression of the HER2 pathway in MCF-7 cells results in downregulation of ER expression and inactivation of ERE-driven reporter transcription[8,9]. The finding that signalling by HRG promotes ligand-independent suppression of ER transcription also supports a link between the HER2 and ER receptor pathways[6–9]. In spite of these findings, the molecular basis of hormone independence and the putative function of these histone modifications remain unexplored.

The eukaryotic genome is compacted with histone and other proteins to form chromatin, which consists of repeating units of nucleosomes[11]. For transcription factors to access DNA, the repressive chromatin structure needs to be remodelled. Dynamic alterations in chromatin structure can facilitate or suppress access of transcription factors to nucleosomal DNA, leading to transcriptional regulation. One way to achieve this is through alterations in the acetylation state of nucleosomal histones[11–13]. Acetylation of core histones occurs at lysine residues on their amino-terminal

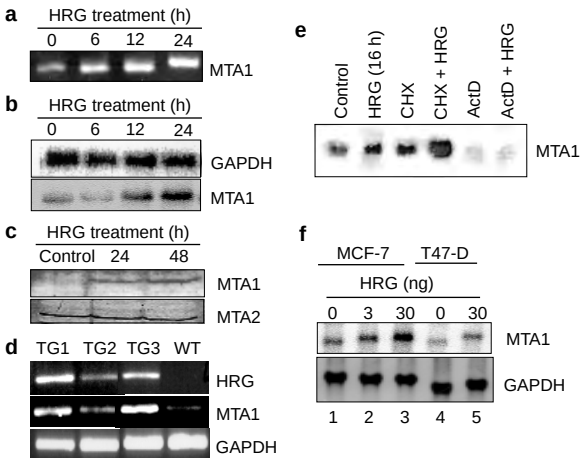

Figure 1 **HRG regulation of MTA1 expression. a**, RT-PCR analysis of MTA1 expression. **b**, Northern-blot analysis of HRG regulation of MTA1 expression in MCF-7 cells. **c**, Western-blot analysis of HRG regulation of MTA1 or MTA2 expression in MCF-7 cells. **d**, RT-PCR analysis of HRG and MTA1 expression in Harderian-gland tumours from HRG transgenic mice. TG1, TG2 and TG3, Harderian-gland tumours from HRG transgenic mice. WT, wild-type mice. **e**, Regulation of MTA1 mRNA by HRG in MCF-7 cells. CHX, cyclohexamide; ActD, actinomycin D. **f**, Dose-dependent upregulation of MTA1 mRNA in MCF-7 cells (lanes 1–3) and T47-D cells (lanes 4 and 5); $n = 3$.

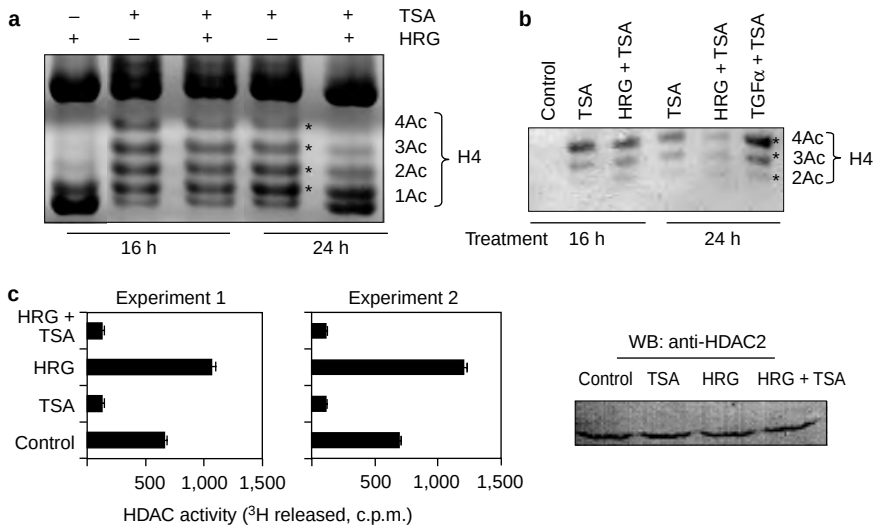

Figure 2 **HRG regulation of HDAC activity. a**, Urea–polyacrylamide-gel analysis of histone H4 acetylation in TSA-treated MCF-7 cells in the presence or absence of HRG. **b**, Western-blot analysis of histone H4 acetylation using an antibody against acetylated H4. **c**, Regulation of TSA-sensitive deacetylase activity by HRG in MCF-7 cells. TSA, 300 nM; HRG, 1 nM; *n* = 4. WB, western blot.

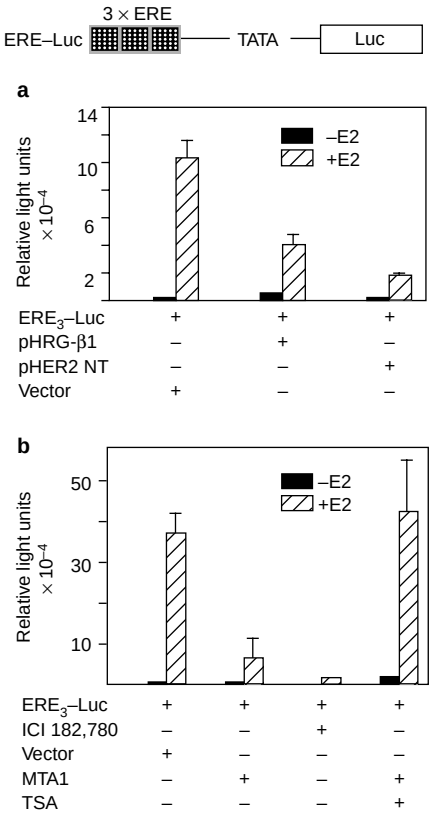

Figure 3 **MTA1 represses ERE-mediated transcription. a**, Repression of 17β-oestradiol (10^{-9} M)-mediated stimulation of ERE–luciferase activity in MCF-7 cells by heregulin gene (pHRGβ1) and point-mutated HER2 (pHER2NT). Shown above is a schematic representation of the ERE–Luc construct. **b**, MCF-7 cells were transfected with ERE–Luc in the presence or absence of MTA1. Where indicated, cultures were treated with TSA (300 nM); *n* = 3.

tails, thus neutralizing the positive charge of the histone tails and reducing their affinity for DNA. Hyperacetylated chromatin is generally associated with transcriptional activation, whereas hypoacetylated chromatin is associated with transcriptional repression[14]. The acetylation state of histones is regulated by a dynamic interaction of two groups of recently identified enzymes — histone acetyltransferases (HATs) and HDACs. HATs and HDACs thus constitute important links between chromatin structure and transcription outcome.

Several recent studies have raised the possibility of a close connection between HDACs and cancer. As HDAC-mediated deacetylation of nucleosomal histones is known to be associated with transcriptional repression of some genes, it has been proposed that deregulation of HDAC recruitment to specific promoters is a potential mechanism by which these HDACs contribute to tumorigenesis. Several recent findings[15–18], which have revealed the identity of a polypeptide (NuRD-70) of nucleosome remodelling and HDAC complex with that of MTA1 have indicated a possible function of HDACs in tumour progression. MTA1 also physically interacts with HDAC1 (ref. 19). The MTA1 gene was originally identified by differential expression in rat mammary adenocarcinoma metastatic cells, and has since been shown to correlate well with the metastatic potential of several human cell lines and tissues[20–22].

Although MTA1 has been shown to be a part of the HDAC complex, the nature of its target or targets remains unidentified. As one of the mechanisms by which hormone independence by HRG is developed includes repression of the ER pathway, and as MTA1 is a component of the HDAC complex, we explored the hypothesis that HRG regulates expression of MTA1, which, as a part of the HDAC complex, may antagonize the activation of the ER pathway by oestradiol. Here we provide new evidence that MTA1 is a target of HRG and represses ER-mediated transcription by recruiting HDACs.

Results

HRG stimulation of MTA1 expression in breast-cancer cells. Because deregulation of the HRG pathway into ER-positive breast-cancer cells leads to suppression of ER-driven transcription[9], and because MTA1 is a component of the HDAC complex[15–18], we initially investigated whether HRG could upregulate the expression of

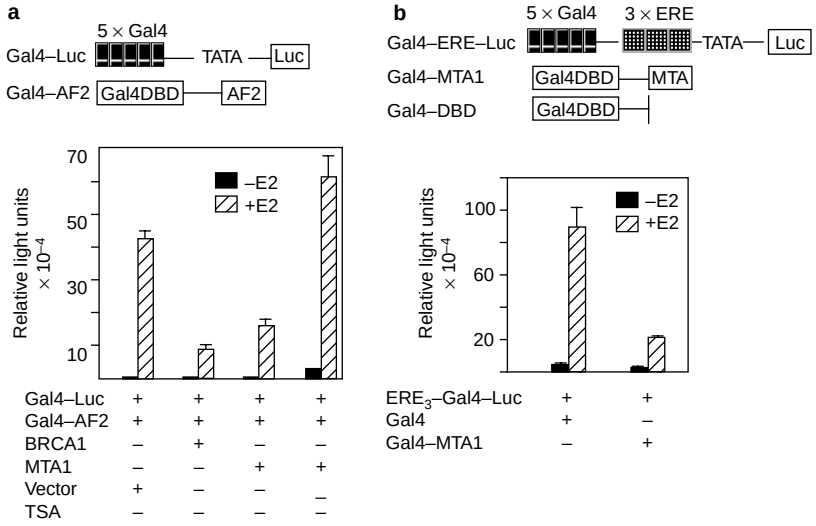

Figure 4 **MTA1 regulation of the function of the ER AF2 domain. a**, MCF-7 cells were co-transfected with Gal4–AF2 and Gal4–Luc (each containing five copies of the Gal4-binding domain) with or without MTA1. BRCA1 was used as a positive control to show its suppression. **b**, E2-dependent direct interactions between Gal4–MTA1 and ERE_3–Gal4–Luc (n = 4). Schematic representations of the constructs used are shown at the top.

MTA1. Using a pair of specific MTA1 primers[20], analysis of RNAs from breast cancer MCF-7 cells by polymerase chain reaction with reverse transcription (RT-PCR) revealed time-dependent stimulation of MTA1 messenger RNA by HRG (Fig.1a). We confirmed the identity of the amplified MTA1 band by sequencing and Southern blotting (data not shown). Using a 291-base-pair PCR probe for MTA1, northern blotting showed a significant increase in steady-state levels of 2.9-kilobase (kb) mRNA for MTA1 in a time-dependent manner (Fig. 1b). Western blotting with an anti-MTA1 antibody[23] also showed that the level of MTA1 of relative molecular mass 80,000 (M_r 80K) was significantly increased in HRG-treated MCF-7 cells (Fig. 1c). HRG had no effect on expression of MTA2 protein. As treatment with HRG for 12 h had no effect on the levels of thymidine incorporation into DNA, or on the cell-cycle distribution of this incorporation (data not shown), the observed effect of HRG on MTA1 expression may not be reflective of the proliferative status of the cell. To evaluate HRG modulation of MTA1 *in vivo*, we used a mouse mammary tumour virus (MMTV)-promoter-driven HRG-transgenic mouse line, which develops mammary adenocarcinomas and Harderian-gland tumours[24]. As Harderian-gland tumours are usually detected by 3 weeks of age, as opposed to 12–16 months for mammary-gland tumours, we used the presence of Harderain-gland tumours to establish the proof-of-principle of our hypothesis *in vivo*. Expression of HRG transgene in Harderian-gland tumours in a MMTV/HRG transgenic mouse model[24] was accompanied by increased expression of MTA1 (Fig. 1d). Treatment of cultures with actinomycin D, an inhibitor of transcription, completely inhibited HRG-mediated induction of MTA1 mRNA (Fig. 1e). Treatment of cells with cycloheximide stabilized the levels of MTA1 mRNA expression; treatment with HRG, however, superinduced the expression of MTA1 mRNA. Induction of MTA1 expression by HRG was also dose-dependent (Fig. 1f). To confirm that MTA1 is expressed in mammary epithelium cancer cells, we also cloned the full-length MTA1 complementary DNA from the human mammary gland cDNA library (data not shown).

Suppression of histone acetylation in HRG-treated cells. As MTA1, a component of the NuRD complex, was induced by HRG, we next examined the influence of HRG on the status of histone acetylation. We treated MCF-7 cells for 16 or 24 h with or without HRG in the presence or absence of trichostatin-A (TSA), a specific HDAC inhibitor, and evaluated the status of histone acetylation using acetic acid–urea–acrylamide gels. Addition of TSA to control cells

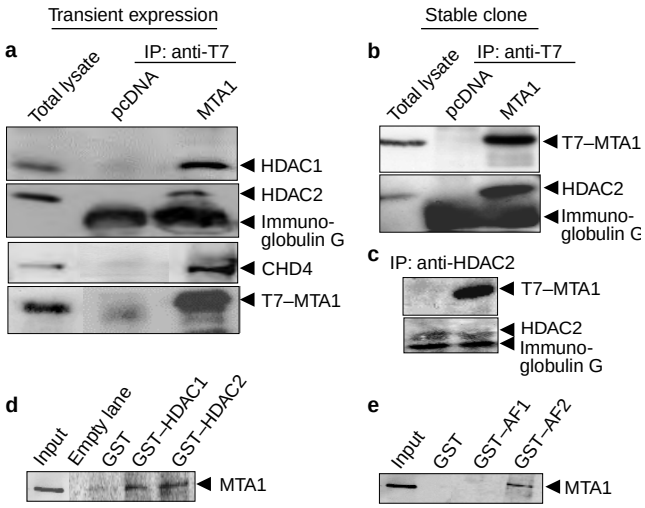

Figure 5 **Direct association of MTA1 with HDACs and ER. a**, MTA1 interacts with HDAC complexes *in vivo*. MCF-7 cells were transiently transfected with T7–MTA1 or control vector. Immunoprecipitation (IP) was carried out using anti-T7 monoclonal antibody; western blotting was carried out with the indicated antibodies. **b**, **c**, T7–MTA1 associates with HDAC2 in the stable cell lines. Cell extracts were immunoprecipitated with anti-T7 antibody, and the same blot was immunoblotted with anti-HDAC2 and anti-T7 antibodies (**b**). In a reverse experiment, extracts were immunoprecipitated with anti-HDAC2 antibody and immunoblotted with anti-T7 and anti-HDAC2 antibodies (**c**). **d**, MTA1 directly interacts with HDAC. GST pull-down assay, showing the association of HDAC with *in vitro*-translated MTA1. **e**, GST pull-down assay, demonstrating a direct interaction between MTA1 and the ligand-binding domian (AF2) of ER (n = 4).

was accompanied by an expected increase in the acetylation of histone 4 (H4, Fig. 2a). However, HRG treatment for longer than 16 h suppressed the levels of H4 acetylation, particularly on bands 4 and 3 (Fig. 2a). Similar results were obtained for cell lysates from the above experiment when immunoblotted with an anti-H4 antibody (Fig. 2b). However, this antibody predominantly recognized acetylated

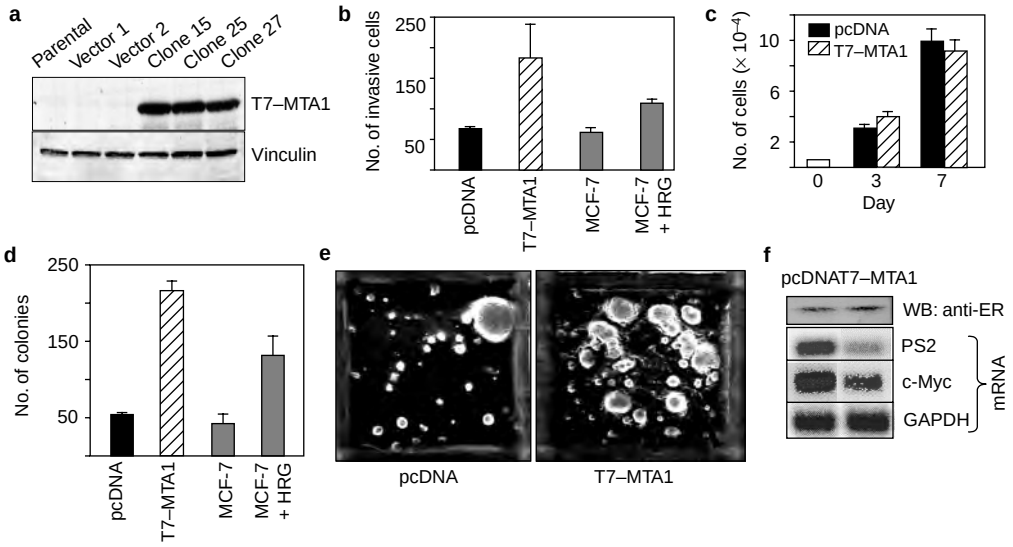

Figure 6 **Characterization of MCF-7 cells overexpressing MTA1. a**, Western-blot analysis of control and T7–MTA1-expressing clones, using anti-T7 monoclonal antibody. The blot was reprobed with anti-vinculin antibody as a loading control. **b**, Invasiveness of MCF-7 cells expressing T7–MTA1 (clone 15) or control vector pcDNA. As a positive reference control for comparison, MCF-7 cells were treated with HRG and another group was left untreated. **c**, Effect of T7–MTA1 expression on the growth rate of cells, as shown by MTT assay. **d**, Effect of T7–MTA1 expression on anchorage-independent growth of MCF-7 cells. As a positive control, MCF-7 cells were treated with HRG and another group was left untreated. **e**, Representative photographs of soft-agar colonies of the indicated strains. **f**, Expression of ER protein and pS2, c-Myc and GAPDH mRNAs in MCF-7 cells expressing vector or T7–MTA1 (n = 3). WB, western blot.

H4 bands 4, 3 and 2 (in decreasing order). This was a specific effect of HRG, as another growth factor, TGF-α, produced no such inhibitory effect (Fig. 2b). HRG treatment of MCF-7 cells was also accompanied by an enhancement of TSA-sensitive HDAC activity without any effect on expression of HDAC2 protein (Fig. 2c). These findings indicate that HRG may interfere with the acetylation of H4, presumably through stimulation of MTA1 expression.

Repression of ERE-mediated transcription by MTA1. Because MTA1 has been shown to be a component of the NuRD complex and to have HDAC activity[15–18], and because HRG induces MTA1 expression as well as histone deacetylation, we hypothesized that MTA1, in conjunction with HDAC complexes, may repress ERE transcription and may thus provide a molecular explanation for the reported suppression of the ER pathway by HRG[7,8]. As shown in Fig. 3a, co-transfection of ERE–luciferase with either HRG or activated (point-mutated) HER2, but not with control vector, was accompanied by significant suppression of ERE–reporter transcription, indicating the possible existence of crosstalk between the HER2/HRG and ER pathways.

To investigate whether HRG-inducible MTA1 serves as specific corepressor of ERE transcription, we repeated the above experiment with MTA1 expression vector. Transient expression of MTA1 effectively blocked the ability of oestradiol to stimulate ERE transcription (Fig. 3b). The inhibitory effect of MTA1 on ERE transcription was antagonized by TSA, a specific inhibitor of HDAC enzyme, indicating that MTA1 potentially recruits HDAC to repress ERE-mediated transcription.

We next examined the recruitment of MTA1 complex(es) to ER elements, using a Gal4–ER/Gal4–Luc assay system[25,26]. This system involves transient transfection of two plasmids, Gal4–AF2 (the ligand-binding domain of ER-α) and Gal4–luciferase reporter; luciferase activation depends on E2 stimulation of the AF2 domain. As shown in Fig. 4a, E2-mediated activation of the AF2 domain could also be repressed by MTA1 expression, and this repression was relieved by TSA. These observations indicate that the observed MTA1 regulation of AF2 function may be independent of the DNA-binding activity of ER and that this may involve HDACs. Many repressors have been shown to repress transcription of specific promoters when recruited by heterologous DNA-binding domain[15,16]. To confirm further the function of MTA1 in ERE transcription, we constructed a reporter gene containing five Gal4 sites placed in front of three ERE sites, and used the GAL4 DNA-binding domain fused MTA1 to recruit MTA1 to the ERE promoter. Expression of Gal4–MTA1 repressed the E2-mediated activity of ERE by up to 80% (Fig. 4b). The repressing effect of MTA1 on the ERE-mediated transcription was not restricted to the ER, as MTA1 also effectively blocked the activation of GRE-mediated transcription by progestin and dexamethasone in a TSA-sensitive manner (see Supplementary Information). Overall, these results establish a new function of MTA1 in repression of the ERE- and GRE-mediated transcription.

Association of MTA1 with HDAC and ER. To determine whether the observed repression of ERE transcription by MTA1 was associated with recruitment of HDAC complexes *in vivo*, we next examined the association between T7-tagged MTA1 and the components of HDACs by co-immunoprecipitation and western blotting (Fig. 5a). Transient expression of T7-tagged MTA1, but not of control T7 vector, in MCF-7 cells was accompanied by interactions with HDAC1, HDAC2 and chromodomain protein 4 (CHD4). Similar results were also obtained when extracts from the stable cell lines were analysed. As shown in Fig. 5b, immunoprecipitation of the extracts from stable cell lines with anti-T7 antibody (Fig. 5b) or anti-HDAC2 antibody (Fig. 5c) further confirmed the existence of a physical association between HDAC2 and T7-MTA1.

To investigate whether the observed association between MTA1 and HDAC1 or HDAC2 was direct or was mediated through other proteins, we examined the binding ability of *in vitro*-translated MTA1 protein with glutathione-S-transferase (GST)-tagged HDAC1 and HDAC2. MTA1 interacted with GST–HDAC1 and GST–HDAC2, but not with GST alone, in GST pull-down assays (Fig. 5d). A physical interaction has also been reported between MTA1 and HDAC1 (ref. 19).

As MTA1 repressed ERE-mediated transcription by recruiting HDAC, we hypothesized that MTA1 physically interacts with ER to

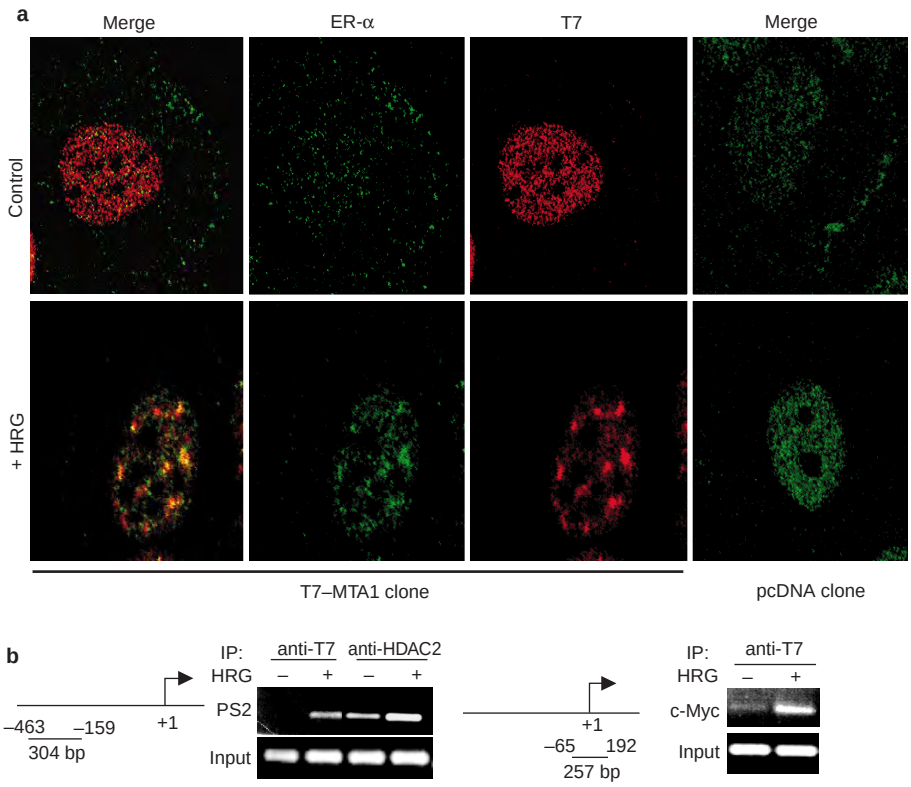

Figure 7 **HRG promotes interaction of MTA1 with the endogenous ER pathway. a**, T7–MTA1 and ER-α partially co-localize in the nuclei of MCF-7 cells expressing T7–MTA1. Confocal images of single optical sections are shown. Double labelling was carried out with a rabbit antibody against human ER-α (green) and a mouse monoclonal antibody against T7 to visualize MTA-1 (red). HRG treatment induced co-localization of ER with T7–MTA1 in large nuclear domains, as shown by the presence of yellow colour in the merged images. **b**, Analysis of MTA1–HDAC2 association on ERE-responsive promoters by chromatin-immunoprecipitation assay. MCF-7 cells were treated with or without HRG (30 ng ml^{-1} for 16 h), and chromatin lysates were immunoprecipitated (IP) with anti-T7 or anti-HDAC2 antibodies; samples were processed as described in Methods. Upper panels of the blots show PCR analysis of pS2 (304 bp) and c-Myc (257 bp) promoter fragments associated with T7–MTA1 or HDAC2 (schematic representations are shown to the left of blots); lower panels show PCR analysis of the DNA input.

influence its function. To explore this possibility, we examined the binding ability of *in vitro*-translated MTA1 with GST-tagged AF1 and AF2 domains of ER in GST pull-down assays. MTA1 protein effectively interacted with GST–AF2 (the ligand-binding domain of ER), but not with GST alone or with GST–AF1 (Fig. 5e). These results support the hypothesis that MTA1 acts as a transcription repressor by recruiting the HDAC complex.

Effect of MTA1 on the biology of breast-cancer cells. To delineate further the potential contribution of MTA1 in breast-cancer cells, we established stable MCF-7 clones expressing T7-tagged MTA1 or control vector (Fig. 6a). For subsequent studies, we used MCF-7 clone 15 expressing T7-MTA1, and control-vector-transfected MCF-7 cells (clone V2). We analysed the influence of MTA1 expression on the invasion of MCF-7 cells using a Boyden chamber. Vector-transfected cells showed low invasiveness (Fig. 6b), whereas expression of MTA1 resulted in a significant increase in cell invasiveness (Fig. 6b). As a positive reference control, we treated MCF-7 cells with HRG, a known inducer of invasiveness in these cells[10], and left another group untreated. To examine the potential influence of MTA1 expression on the growth characteristics of breast epithelial cancer cells, we measured the growth rate and ability of cells to grow in an anchorage-independent manner. Expression of MTA1 had little or no significant effect on the growth rate of MCF-7 cells on plastic (Fig. 6c). However, MTA1 expression significantly enhanced the ability of MCF-7 cells to form colonies on soft agar (Fig. 6d). As a positive control, we treated MCF-7 cells with HRG and left another group untreated. Overexpression of MTA1 was accompanied by a significant, reproducible enhancement of the ability of cells to form larger colonies in soft agar, as compared to those formed by vector-transfected control cells (Fig. 6e). Although MTA1 expression had no effect on the level of ER, MTA1-overexpressing breast-cancer cells exhibited a reduction in the levels of ER target genes, including those encoding pS2 and c-Myc (Fig. 6f). Together, these observations indicate that cells expressing MTA1 may affect the status of ER-responsive genes and that these cells may acquire more invasive phenotypes.

HRG promotes interaction of MTA1 with endogenous ER. Having shown that MTA1 has a role in the invasiveness of breast-cancer cells, we next investigated the effect of HRG on the potential interaction between MTA1 and endogenous ER in MCF-7 cells expressing T7-tagged MTA1 or control vector. We fixed cells treated with or without HRG, co-stained them with antibodies against ER or T7-tag, and quantified the resulting immunofluorescence by laser-scanning confocal microscopy. MTA1 was abundantly present in the nuclei of T7–MTA1-expressing cells, exhibiting a fine granular pattern in untreated control cells (Fig. 7a, upper-left panel; see also Fig. 7a, T7). In contrast, T7–MTA1 was expressed in larger nuclear domains in HRG-treated clones (Fig. 7a, lower-left panel). No positive staining was detected in cell transfected with empty vector (Fig. 7a, right panels). Interestingly, within the larger nuclear domains, MTA1 partially colocalized with ER-α only upon HRG treatment (represented by yellow staining). Very fine serial confocal sectioning revealed that ER staining was dispersed as several smaller nuclear dots decorating the surface of the larger anti-MTA1-

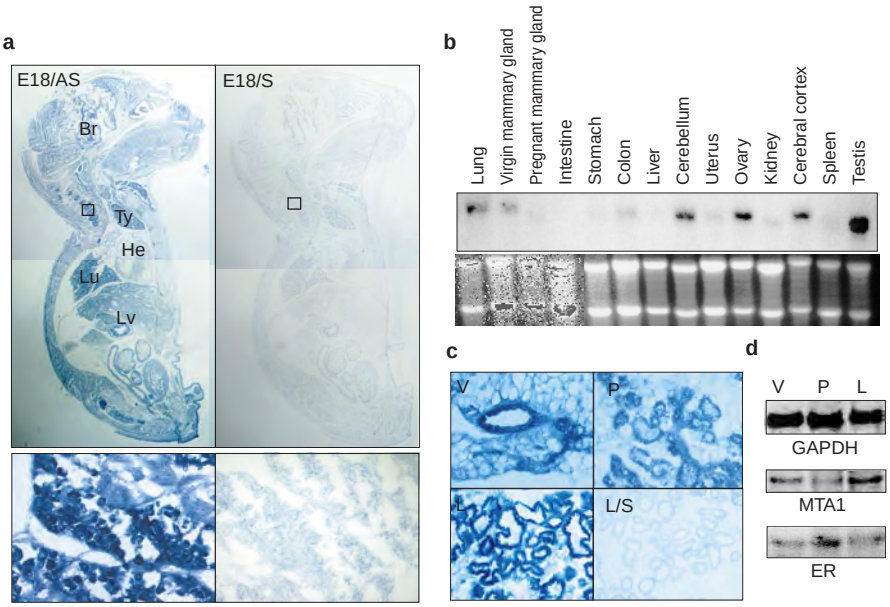

Figure 8 **MTA1 expression during embryogenesis and mammary-gland development. a**, MTA1 expression in an E18 embryo. MTA1 expression was detected by a specific anti-sense MTA1 riboprobe (E18/AS). Sense-probe hybridization was used to show the background staining (E18/S). Br, brain; Lu, lung; Ty, thymus; Lv, liver. Lower panels are enlargements of the boxed areas in the upper panels. **b**, Northern-blot analysis of MTA1 expression in the indicated mouse tissues. **c**, *In situ* hybridization analysis of MTA1 expression. V, virgin mammary gland at day 21; P, pregnant mammary gland at day 15; L, lactating mammary gland at day 12; L/S, control *in situ* hybridization, using the sense MTA1 probe, in lactating mammary gland. **d**, Northern-blot analysis of expression of MTA1 and ER in the samples described in **c** ($n = 2$).

reactive nuclear domains. As shown in Fig. 7a, overexpression of T7–MTA1 was not sufficient to induce a significant increase in the interaction between T7–MTA1 and ER, whereas HRG treatment could rapidly trigger this process. These observations raise the possibility that the observed MTA1–ER interaction may be an indirect effect of HRG, and may potentially involve an unidentified component or components of HRG pathways that lead to MTA1.

HRG treatment induces MTA1–HDAC association on ERE-responsive promoters *in vivo*. To assess directly the potential significance of the physical interaction between MTA1 and ER in HRG-activated cells, we investigated whether MTA1 and HDAC associate on the chromatin of endogenous RE-containing promoters, using a chromatin-immunoprecipitation (ChIP) assay. We treated MCF-7 cells expressing T7-tagged MTA1 with HRG and left another group untreated, and processed them with formaldehyde and sonicated chromatin for immunoprecipitation with specific antibodies against T7 or HDAC2. We analysed genomic DNA fragments bound to T7–MTA1 or to HDAC2 by quantitative PCR using primers spanning ERE elements present in the promoters of the genes encoding pS2 (ref. 27) and c-Myc (ref. 28), to assay for potential HRG-triggered association of T7–MTA1 or HDAC2 with the promoters of two ERE target genes. HRG treatment triggered significant increases in the amount of chromatin from the promoters of both the pS2 and c-Myc genes (5.8- and 4.1-fold, respectively, relative to untreated cells) that was associated with T7–MTA1 (Fig. 7b). Alterations in the amount of HRG-responsive increase of pS2-promoter DNA with HDAC2 were also significant, but less profound (1.8-fold increase relative to untreated cells, Fig. 7b). We repeated these experiments three times with similar results, and have thus demonstrated the potential complexity of regulation of promoter chromatin by multi-protein complexes. As the association of MTA1 with the ERE-responsive promoters of ER target genes was dependent on HRG treatment, the observed effects may involve HRG-triggered cellular events, and hence may be indirect. Together, these findings strongly support the idea that MTA1 interacts with endogenous ER and that both MTA1 and HDAC2 associate with ERE-containing promoters in HRG-treated cells.

Expression of MTA1 during embryogenesis and mammary-gland development. During embryonic development, HDAC may work constantly to control the on/off function of the genes that regulate cell proliferation and differentiation. However, little is known of the expression profile of HDAC components. We investigated MTA1 expression in mouse embryonic development by *in situ* hybridization. As shown in Fig 8a, MTA1 mRNA was expressed in most tissues, with highest levels present in rapidly proliferating tissues such as liver, lung and thymus. MTA1 mRNA signals in the vertebral column, heart and intestinal tract were significantly weaker. At high magnification, MTA1 signals were detected in the cytoplasm of neuronal cells in the cervical neuronal arch (Fig. 8a, lower panels). In accordance with the results of *in situ* hybridization, high levels of MTA1 mRNA expression were detected in the brain, lung and testis; high levels of MTA1 mRNA expression were also detected in the mammary gland by northern blotting of RNAs from several organs from female mice (Fig. 8b).

In situ-hybridization analysis of mouse mammary gland showed that MTA1 mRNA was present in the cytoplasm of virgin ducts, in the growing-end buds of the pregnant mammary gland, and in lactating alveoli (Fig. 8c). The signal was much stronger in the lactating alveoli and the virgin mammary gland than in the pregnant and the involuting mammary gland. Signals from the pregnant mammary gland were relatively weaker. Low levels of MTA1 expression were detected in the virgin fat-pad tissues.

As MTA1 regulates the function of ER in breast-cancer cells, we next examined the expression pattern of MTA1 during mammary-gland development, and the relationship between MTA1 expression and ER expression. The northern-blot analysis showed that MTA1 was expressed during all stages of mammary-gland development (Fig. 8d). The highest levels of MTA1 expression were observed during lactation, when ER levels were lower. These results indicate that MTA1 may regulate the expression of one or more ER target genes, and could influence ER function.

Discussion

We have shown that MTA1 is a target of HRG in breast-cancer cells and that MTA1 represses ER-mediated transcription by recruiting HDACs. Recruitment of HDAC to promoters has emerged as a general mechanism of transciption repression of target genes. For example, recruitment of HDAC complex to target genes of the retinoic-acid receptor represses transcription and prevents differentiation, and treatment with retionic acid induces differentiation by displacing HDAC complex from PML–RAR-α (refs 29, 30). Similarly, transcription-repressor complexes containing HDAC have been discovered in the RB/E2F[31] and Myc/Mad (reviewed in ref. 32) pathways. Recruitment of HDACs to specific promoters may be mediated either through direct interactions with regulatory proteins such as transcription factor YY1 (ref. 33), or through interaction with corepressors containing an HDAC-interacting domain, such as Sin3A. Nuclear hormone receptors have been shown to bind to the corepressor N-CoR, which directly interacts with the Sin3A–HDAC corepressor complex[16].

Our observation that MTA1 can directly interact with HDAC1/2 and the AF2 domain of ER is important because it indicates that the reported association between MTA1 and HDACs in the NuRD complex[15–18] may reflect direct MTA1 interaction. In addition, we have identified specific nuclear targets and a corepressor function for MTA1, as it effectively suppressed ligand-induced activation of ER.

Expression of MTA1 correlates well with the metastasis potential of several human cancer cell lines and tissues[20–22]. However, direct evidence to link enhanced MTA1 expression with metastasis is currently lacking. MTA1 has been found to contain a domain (known as the WFY domain) that is similar to two regions of N-CoR[17]. The WFY domain of MTA1 is less likely to be involved in recruiting HDACs in our system, because we detected no appreciable interaction between MTA1 and N-CoR (data not shown). However, specific domains of MTA1 may directly associate with both HDAC2 and AF-2 (Fig. 5c). In summary, we have identified ER-mediated transcription as a nuclear target of corepressor MTA1, and have provided new evidence to support the idea that HDAC complexes are involved in MTA1-mediated transcriptional repression of oestrogen. □

Methods

Cell culture, transfection, cell extracts and reagents.

Breast-cancer MCF-7 cells[10] were maintained in DMEM–F12 (1:1 ratio) supplemented with 10% FCS. Cell lysates were prepared as described[10] and were resolved on a 10% SDS–polyacrylamide gel, transferred to nitrocellulose, and probed with the appropriate antibodies. Antibodies against HDAC1 and HDAC2 were from Santa Cruz; anti-T7 antibody was from Novagen. Transfection was carried out using the Fugene-6 kit (Roche) according to the manufacturer's instructions.

Northern blotting and promoter–reporter assays.

Total cytoplasmic RNA (20 μg) was analyzed by northern blotting[10]. For promoter assays, cells were transiently co-transfected with a reporter construct and β-galactosidase. Cells were collected with passive lysis buffer or were processed for CAT assay (Promega).

Construction of reporter systems.

3 × ERE–TATA–luciferase plasmid was from D. McDonnell (Duke Univ., Durham, North Carolina). 5 × GAL4 plasmid was from F. Claret, M. D. Anderson Cancer Center. Full-length MTA1 cDNA was isolated from a human mammary gland cDNA library (Invitrogen). MTA1 cDNA containing the entire reading frame of MTA1 was subcloned into pcDNA3.1–T7 vector using restriction sites *Eco*RI and *Xba*I to generate T7-tagged MTA1. To construct 5 × Gal4–ERE–luciferase construct, 5 × Gal4 sites were isolated by PCR using Gal4 5 × luciferase as a backbone (*Sma*I and *Kpn*I sites were added to primers) and subcloned into *Sma*I and *Kpn*I sites of 3 × ERE–TATA–luciferase plasmid. The identities of constructs were verified by sequencing.

In vitro transcription and translation.

In vitro transcription and translation of MTA1 proteins was carried out using the TNT transcription–translation system (Promega). MTA1 cDNA (1 μg) in pcDNA 3.1 vector was *in vitro* translated in the presence of [^{35}S]methionine in a reaction volume of 50 μl using the T7–TNT kit (Promega). The reaction was diluted to 1 ml with NP40 lysis buffer; an aliquot (250 μl) was used for each GST pull-down assay. Translation was verified by subjecting 2 μl of the reaction mixture to SDS–PAGE and autoradiography.

Histone–urea gels and deacetylase assays.

Histones were purified and resolved onto a 15% urea gel as described[34]. HDAC activity was measured by scintillation counting of [^{3}H]acetic acid released from ^{3}H-acetylated histones as described[17].

GST pull-down assay.

GST pull-down assays were carried out by incubating equal amounts of GST, GST–AF1, GST–AF2, GST–HDAC1 or GST–HDAC2 immobilized on glutathione–sepharose beads (Amersham) with *in vitro*-translated ^{35}S-labelled MTA protein. The mixture was incubated for 2 h at 4 °C and washed with NP40 lysis buffer; bound proteins were eluted with 2 × SDS buffer, separated by SDS–PAGE and developed by fluorography[35].

Production of stable cell lines expressing MTA1.

MCF-7 cells were transfected with pcDNA3.1 or pcDNA.T7–MTA1 using the calcium-phosphate method. Forty-eight hours after transfection, cells were selected in media containing 1 mg ml^{-1} G418. Several individual clones were isolated and expanded, and expression of exogenous MTA1 was verified by immunoblotting using anti-T7 monoclonal antibody.

Cell-proliferation, invasion and soft-agar assays.

Cell-invasion assays were carried out using Boyden chambers as described[36]. Cells were plated on the upper well of a Boyden chamber at a concentration of 20,000 cells per well. The lower side of the separating filter was coated with chemoattractant (thick layer of a 1:2 dilution of Matrigel (Life Technologies)) in serum-free medium. The number of cells that successfully migrated through the filter and invaded the 2-mm Matrigel layer, as well as those that remained on the upper side of the filter, were counted after staining with propidium iodide (Sigma). The percentage of the total number of cells that migrated was recorded; data are means ± s.e.m. from triplicate wells in three separate experiments.

Cell-proliferation assays were carried out using the 3-(4,5-dimethyl-thiazol-2-yl)diphenyltetrazolium bromide (MTT) dye method as described[8,10]. Soft-agar colony-growth assays were carried out as described[37]. Briefly, 1 ml of 0.6% DIFCO agar in DMEM supplemented with 10% FBS and insulin was layered onto 60 × 15-mm tissue-culture plates. MCF-7 cells (10,000 cells) were mixed with 1 ml of 0.36% Bactoagar solution in DMEM prepared in a similar manner and layered on top of the 0.6% Bactoagar layer. Plates were incubated at 37 °C in 5% CO_2 for 21 days.

Immunofluorescence confocal studies.

Cellular localization of T7–MTA1 and ER was determined using indirect immunofluorescence as described[10]. Briefly, cells grown on glass coverslips were fixed (without permeabilization) in ethanol/methanol (1:1) at –20 °C for 3 min. Cells were treated with or without anti-T7 monoclonal antibody or anti-ER antibody and were then treated with Alexa-546-labelled goat anti-mouse antibody or Alexa-488 (Molecular Probes). For controls, cells were treated only with the secondary antibodies. Images are z-sections taken at the same cellular level and magnification. Confocal analysis was carried out using a Zeiss laser-scanning confocal microscope and the established methods, involving processing of the same section for each detector (two excitations corresponding to 546 and 488 nm) and comparing images pixel by pixel. Co-localization of the two proteins is indicated by the presence of yellow color as a result of overlapping red and green pixels.

Chromatin immunoprecipitation (ChIP) assays.

Quantitative ChIP assays were carried out as described[38,39]. Cells were treated with 37% formaldehyde solution (final concentration 1%) to crosslink T7–MTA1 or HDAC2 to DNA. Cells were washed twice with PBS (pH 7.4) containing protease-inhibitor cocktail (Roche) and were then lysed with lysis buffer containing 1% SDS and sonicated as described[38]. Supernatants from sonicated lysates were diluted ten-fold with chromatin-dilution buffer containing 0.01% SDS, 1.1% Triton X-100 and protease-inhibitor cocktail. For input DNA, 1% of the chromatin solution was kept aside before immunoprecipitation. Chromatin solutions were immunoprecipitated with anti-T7 (Novagen) or anti-HDAC2 antibody (Santa Cruz) at 4 °C overnight. Beads were washed as described[1] on a rotating platform before finally eluting antibody-bound chromatin by incubation with 400 μl of 1% SDS containing 0.1 M $NaHCO_3$. The eluate, as well as the input chromatin, was heated to 65 °C for 6 h to reverse the formaldehyde crosslinks, and was then subjected to phenol-chloroform extraction. The supernatant was ethanol-precipitated and resuspended in 50 μl of 10 mM Tris–1 mM EDTA, pH 7.4. Quantitative PCR analysis was carried out with 10 μl of DNA sample restricted to 25 cycles. Our pS2 gene primers[27] amplify the region including the ER-responsive element from position –463 to –159; c-Myc gene primers[28] amplify the region from –65 to +192. PCR products were resolved on 1.5% agarose gel and visualized with ethidium bromide. Images were quantified using Sigma gel-analysis software, version 1.

In situ hybridization.

For *in situ* hybridization, mouse mammary-gland tissues or 18-day-old embryos (E18) were cut out and fixed with 10% neutral-buffered formaldehyde and processed routinely to make paraffin sections as described[40]. *In situ* hybridization was carried out in frozen sections using the digoxigenin-labelled riboprobe (Roche). A 290-bp fragment of mouse MTA1 cDNA corresponding to bases 1,781–2,070 of the human MTA1 mRNA region was amplified by RT-PCR, subcloned into the TOPO II vector (Promega) and used for riboprobe synthesis. RNA probes were labelled with digoxigenin and hybridized for 16–20 h in buffer containing 1 μg ml^{-1} riboprobes, 50% formamide, 300 mM NaCl, 10 mM Tris pH 7.4, 10 mM NaH_2PO_4 pH 6.8, 5 mM EDTA pH 8.0, 0.2% Ficoll 400, 0.2% polyvinyl pyrolidone, 10% dextran sulphate, 200 μg ml^{-1} yeast total RNA and 50 mM dithiothreitol. Alkaline-phosphatase-labelled sheep anti-digoxigenin antibody was applied and signals were visualized by NBT-BCIP. Sense-probe hybridization was used for background control.

RECEIVED 15 MAY 2000; REVISED 14 AUGUST 2000; ACCEPTED 18 SEPTEMBER 2000; PUBLISHED 6 DECEMBER 2000.

1. Nass, S. J. & Davidson, N. E. The biology of breast cancer. *Hematol. Oncol. Clin. N. Am.* **13,** 311–332 (1999).
2. Muss, H. B. *et al.* c-erbB-2 expression and response to adjuvant therapy in women with node-posi-

tive early breast cancer. *N. Engl. J. Med.* **330,** 1260–1266 (1994).
3. Borg, A. *et al.* ERBB2 amplification is associated with tamoxifen resistance in steroid-receptor positive breast cancer. *Cancer Lett.* **81,** 137–144 (1994).
4. Wright, C. *et al.* Relationship between c-erbB-2 protein product expression and response to endocrine therapy in advanced breast cancer. *Br. J. Cancer* **65,** 118–121 (1992).
5. Benz, C. C. *et al.* Estrogen-dependent, tamoxifen-resistant tumorigenic growth of MCF-7 cells transfected with HER2/neu. *Breast Cancer Res. Treat.* **24,** 85–95 (1995).
6. Hynes, N. C. & Stern, D. F. The biology of erbB-2/neu/HER-2 and its role in cancer. *Biochim. Biophys. Acta* **1198,** 165–184 (1994).
7. Pietras, R. J. *et al.* HER-2 tyrosine kinase pathway targets estrogen receptor and promotes hormone-independent growth in human breast cancer cells. *Oncogene* **10,** 2435–2446 (1995).
8. Kumar, R., Mandal, M., Ratzkin, B. J., Liu, N. & Lipton, A. NDF induces expression of a novel 46 kD protein in estrogen receptor positive breast cancer cells *J. Cell. Biochem.* **62,** 102–112 (1995).
9. Tang, C. K. *et al.* Involvement of heregulin-beta2 in the acquisition of the hormone-independent phenotype of breast cancer cells. *Cancer Res.* **56,** 3350–3358 (1996).
10. Adam, L. *et al.* Heregulin regulates cytoskeletal reorganization and cell migration through the p21-activated kinase-1 via phosphatidylinositol-3 kinase. *J. Biol. Chem.* **273,** 28238–28246 (1998).
11. Owen-Hughes, T. & Workman, J. L. Experimental analysis of chromatin function in transcription control. *Crit. Rev. Eukaryot. Gene. Expr.* **4,** 403–441 (1994).
12. Owen-Hughes, T., Utley, R. T., Cote, J., Peterson, C. L. & Workman, J. L. Persistent site-specific remodeling of a nucleosome array by transient action of the SWI/SNF complex. *Science* **273,** 513–516 (1996).
13. Paranjape, S. M., Kamakaka, R. T. & Kadonaga, J. T. Role of chromatin structure in the regulation of transcription by RNA polymerase II. *Annu. Rev. Biochem.* **63,** 265–297 (1994).
14. Brownell, J. E. *et al.* Tetrahymena histone acetyltransferase A: a homolog to yeast Gcn5p linking histone acetylation to gene activation. *Cell* **84,** 843–851 (1996).
15. Hassig, C. A., Fleischer, T. C., Billin, A. N., Schreiber, S. L. & Ayer, D. E. Histone deacetylase activity is required for full transcriptional repression by mSin3A. *Cell* **89,** 341–347 (1997).
16. Laherty, C. D. *et al.* Histone deacetylases associated with the mSin3 corepressor mediate mad transcriptional repression. *Cell* **89,** 349–356 (1997).
17. Xue, Y. *et al.* NURD, a novel complex with both ATP-dependent chromatin-remodeling and histone deacetylase activities. *Mol. Cell* **2,** 851–861 (1998).
18. Zhang, Y. *et al.* Analysis of the NuRD subunits reveals a histone deacetylase core complex and a connection with DNA methylation. *Genes Dev.* **13,** 1924–1935 (1999).
19. Toh, Y. *et al.* Molecular analysis of a candidate metastasis-associated gene, MTA1, possible interaction with histone deacetylase 1. *J. Exp. Clin. Cancer Res.* **19,** 105–111 (2000).
20. Toh, Y., Pencil, S. D. & Nicolson, G. L. A novel candidate metastasis-associated gene, *mta1*, differentially expressed in highly metastatic mammary adenocarcinoma cell lines. cDNA cloning, expression, and protein analyses. *J. Biol. Chem.* **269,** 229–263 (1994).
21. Toh, Y. *et al.* Overexpression of the MTA1 gene in gastrointestinal carcinomas: correlation with invasion and metastasis. *Int. J. Cancer* **74,** 459–463 (1997).
22. Toh, Y., Kuwano, H., Mori, M., Nicolson, G. L. & Sugimachi, K. Overexpression of metastasis-associated MTA1 mRNA in invasive oesophageal carcinomas. *Br. J. Cancer* **79,** 1723–1726 (1999).
23. Kleene, R., Zdzieblo, J., Wege, K. & Kern, H-F. A novel zymogen granule protein (ZG29p) and the nuclear protein MTA1p are differentially expressed by alternative transcription initiation in pancreatic acinar cells of the rat. *J. Cell Sci.* **112,** 2539–2548 (1999).
24. Krane, I. M. & Leder, P. NDF/heregulin induces persistence of terminal end buds and adenocarcinomas in the mammary glands of transgenic mice. *Oncogene* **12,** 1781–1788 (1996).
25. Henttu, P. M., Kalkhoven, E. & Parker, M. G. AF-2 activity and recruitment of steroid receptor coactivator 1 to the estrogen receptor depend on a lysine residue conserved in nuclear receptors. *Mol. Cell. Biol.* **17,** 1832–1839 (1997).
26. Fan, S. *et al.* BRCA1 inhibition of estrogen receptor signaling in transfected cells. *Science* **284,** 1354–1356 (1999).
27. Berry, M., Nunez, A. M. & Chambon, P. Estrogen-responsive element of the human pS2 gene is an imperfectly palindromic sequence. *Proc. Natl Acad. Sci USA* **86,** 1218–1222 (1989).
28. Dubik, D. & Shiu, R. P. C. Mechanism of estrogen activation of c-myc oncogene expression. *Oncogene* **7,** 1587–1594 (1992).
29. Lin, R. J. *et al.* Role of the histone deacetylase complex in acute promyelocytic leukaemia. *Nature* **391,** 811–814 (1998).
30. Grignani, F. *et al.* Fusion proteins of the retinoic acid receptor-alpha recruit histone deacetylase in leukaemia. *Nature* **391,** 815–818 (1998).
31. Brehm, A. *et al.* Retinoblastoma protein recruits histone deacetylase to repress transcription. *Nature* **391,** 597–601 (1998).
32. Kouzarides, T. Histone acetylases and deacetylases in cell proliferation. *Curr. Opin. Genet. Dev.* **9,** 40–48 (1999).
33. Yang, W. M., Inouye, C., Zeng, Y., Bearss, D. & Seto, E. Transcriptional repression by YY1 is mediated by interaction with a mammalian homolog of the yeast global regulator RPD3. *Proc. Natl Acad. Sci. USA* **93,** 12845–12850 (1996).
34. Boffa, L. C., Vidali, G., Mann, R. S. & Allfrey, V. G. Suppression of histone deacetylation *in vivo* and *in vitro* by sodium butyrate. *J. Biol. Chem.* **253,** 3364–3366 (1978).
35. Yang, W. M., Yao, Y. L., Sun, J. M., Davie, J. R. & Seto, E. Isolation and characterization of cDNAs corresponding to an additional member of the human histone deacetylase gene family. *J. Biol. Chem.* **272,** 28001–28007 (1997).
36. Adam, L., Vadlamudi, R., Mandal, M., Chernoff, J. & Kumar, R. Regulation of microfilament reorganization and invasiveness of breast cancer cells by p21-activated kinase-1 K299R. *J. Biol. Chem.* **275,** 12041–12050 (2000).
37. Vadlamudi, R. *et al.* Regulatable expression of p21-activated kinase-1 promotes anchorage-independent growth and abnormal organization of mitotic spindles in human epithelial breast cancer cells. *J. Biol. Chem.* **275,** 36238–36244 (2000).
38. Braunstein, M., Rose, A. B., Holmes, S. G., Allis, C. D. & Broach, J. R. Transcritional silencing in yeast is associated with reduced nucleosome acetylation. *Genes Dev.* **7,** 592–604 (1993).
39. Hecht, A., Strahl-Bolsinger, S. & Grunstein, M. Spreading of transcriptional repressor SIR3 from telomeric heterochromatin. *Nature* **383,** 92–96 (1996).
40. Wang, R. A. & Zhao, G. Q. Transforming growth factor beta signal transducer Smad2 is expressed in mouse meiotic germ cells, Sertoli cells, and Leydig cells during spermatogenesis. *Biol. Reprod.* **61,** 999–1004 (1999).

ACKNOWLEDGEMENTS

We thank D. Allies for anti-acetylated H4 antibody, D. McDonnell for 3X-ERE TATA, P. Leder for heregulin transgenic mice, F. Claret for 5XGAL4, W. Wang for Gal4–MTA1 and anti-CHD4 antibody, D. Shapiro for ERE-reporter systems, M. R. Parker for AF1 and AF2 fusion-protein expression vectors, E. Seto for HDACs expression vectors, S. Roth for HDAC assay substrate and useful tips, D. Stern for HER2 constructs, M-C. Hung for the Gal4 system, W. Schmid for GRE–CAT promoter constructs, R. Kleene for anti-MTA1 antibody, and D. Reinberg for anti-MTA2 antibody. This study was supported by NIH grants CA80066, CA65746 and CA84456, by the Breast Cancer Research Program of The University of Texas M. D. Anderson Cancer Center (to R.K.), and by Cancer Center Core grant CA16672.

Correspondence and requests for materials should be addressed to R.K. Supplementary Information is available on *Nature Cell Biology*'s website (http://cellbio.nature.com) or as paper copy from the London editorial office of *Nature Cell Biology*.

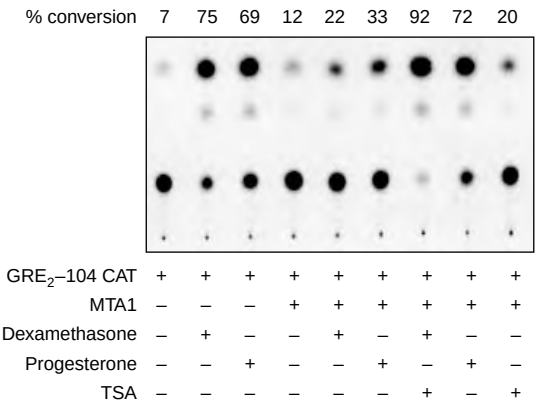

Figure S1 **MTA1 act as a global steroidal repressor.** MCF-7 cells were co-transfected with a GRE–CAT promoter–reporter construct and MTA1 or with a vector control. Some cultures were treated with dexamethasone (500 nM) or progesterone (500 nM) for 16 h, and cell extracts were assayed for CAT activity (n = 4).

Lumefantrine, an antimalarial drug, reverses radiation and temozolomide resistance in glioblastoma

Yetirajam Rajesh[a,b], Angana Biswas[a], Utkarsh Kumar[c], Indranil Banerjee[a], Subhayan Das[a], Santanu Maji[b], Swadesh K. Das[b,d,e], Luni Emdad[b,d,e], Webster K. Cavenee[f,1], Mahitosh Mandal[a,1], and Paul B. Fisher[b,d,e,1]

[a]School of Medical Science and Technology, Indian Institute of Technology, Kharagpur, West Bengal 721302, India; [b]Department of Human and Molecular Genetics, School of Medicine, Virginia Commonwealth University, Richmond, VA 23298; [c]Department of Biotechnology, Indian Institute of Technology, Kharagpur, West Bengal 721302 India; [d]Virginia Commonwealth University (VCU) Institute of Molecular Medicine, School of Medicine, Virginia Commonwealth University, Richmond, VA 23298; [e]VCU Massey Cancer Center, School of Medicine, Virginia Commonwealth University, Richmond, VA 23298; and [f]Ludwig Institute for Cancer Research, University of California San Diego, La Jolla, CA 92093

Contributed by Webster K. Cavenee, March 27, 2020 (sent for review December 9, 2019; reviewed by Antonio Giordano and Jack Greiner)

Glioblastoma multiforme (GBM) is an aggressive cancer without currently effective therapies. Radiation and temozolomide (radio/TMZ) resistance are major contributors to cancer recurrence and failed GBM therapy. Heat shock proteins (HSPs), through regulation of extracellular matrix (ECM) remodeling and epithelial mesenchymal transition (EMT), provide mechanistic pathways contributing to the development of GBM and radio/TMZ-resistant GBM. The Friend leukemia integration 1 (Fli-1) signaling network has been implicated in oncogenesis in GBM, making it an appealing target for advancing novel therapeutics. Fli-1 is linked to oncogenic transformation with up-regulation in radio/TMZ-resistant GBM, transcriptionally regulating HSPB1. This link led us to search for targeted molecules that inhibit Fli-1. Expression screening for Fli-1 inhibitors identified lumefantrine, an antimalarial drug, as a probable Fli-1 inhibitor. Docking and isothermal calorimetry titration confirmed interaction between lumefantrine and Fli-1. Lumefantrine promoted growth suppression and apoptosis in vitro in parental and radio/TMZ-resistant GBM and inhibited tumor growth without toxicity in vivo in U87MG GBM and radio/TMZ-resistant GBM orthotopic tumor models. These data reveal that lumefantrine, an FDA-approved drug, represents a potential GBM therapeutic that functions through inhibition of the Fli-1/HSPB1/EMT/ECM remodeling protein networks.

glioblastoma | HSPB1 | Fli-1 | radioresistance | TMZ resistance

Major pathological features that impose impediments to the management of glioblastoma (GBM) include infiltrative growth behavior, intratumoral heterogeneity, and propensity for tumor recurrence (1–5). Conventional approaches using radiation and temozolomide (TMZ; chemotherapy) have proven unsuccessful in treating GBM because of acquired therapeutic resistance and eventual disease recurrence. Unraveling the molecular mechanisms involved in GBM development and progression provide a potential path forward for developing effective GBM therapies (1, 3, 5). Omics studies in GBM have reported elevated expression of heat shock proteins (HSPs) (1, 6) that promote tumor growth by activating GBM cell proliferation and inhibiting death pathways (1). A positive correlation exists between HSP expression and ECM remodeling that contributes to the infiltrative potential of GBM via binding to MMPs (7). The HSPs also facilitate epithelial-mesenchymal transition (EMT) in cancer (6). Up-regulation of HSPs is evident in GBM and radiation (radio)/TMZ-resistant GBM (6, 8). In these contexts, HSPs provide prospective targets that may be amenable for developing improved clinical strategies for anti-GBM drug development.

HSPB1 is the most up-regulated HSP in GBM and radio/TMZ-resistant GBM (8). Progression and acquisition of radio/TMZ resistance in GBM correlates with elevated expression of HSPB1 mediated through the Ets family of transcriptional regulator(s) (8). In GBM, previous studies confirm a link between hypoxia and up-regulation of HSP expression (9, 10) and regulation of hypoxia and HSPB1 by Ets family proteins (11, 12). Additional evidence in multiple cancer indications highlight important connections between HSPB1 and the Ets family of transcription factors (12–16). The 5-kb upstream region of the HSPB1 gene contains genomic elements that bind to the Friend leukemia integration factor 1 (Fli-1) (8). A member of the ETS family, Fli-1 is a target of insertional activation by Friend murine leukemia virus (F-MuLV) (17). It is expressed in vascular endothelial cells and hematopoietic tissues (18), affecting cellular proliferation and tumorigenesis in Ewing sarcoma and primitive neuroectodermal tumors (13–16, 19, 20). Several oncology studies have reported Fli-1 overexpression as a cancer biomarker (21–25). The present study now defines a relationship between Fli-1 protein and HSPB1 expression that correlates with radio/TMZ resistance in GBM.

Based on the connection between Fli-1 expression and radio/TMZ resistance in GBM cells (8), we screened for Fli-1 inhibitors and identified an antimalarial FDA-approved drug, lumefantrine, as a putative therapeutic agent targeting radio/TMZ resistance in GBM. We have scrutinized the therapeutic actions of lumefantrine in vitro using parental, radioresistant, and TMZ-resistant GBM and in vivo using U87MG orthotopic parental, radioresistant, and TMZ-resistant GBM models. We also endeavored to assess the molecular interactions of lumefantrine with Fli-1 signaling axes, EMT (β-catenin, vimentin, and Snail) and ECM (MMP-2 and MMP-9) remodeling, and apoptosis. In

Significance

No current therapies prevent recurrence in patients with glioblastoma multiforme (GBM). Extracellular matrix (ECM) remodeling and epithelial mesenchymal transition (EMT) are important processes regulating GBM progression and acquisition of radiation and temozolomide (radio/TMZ) resistance. Fli-1 choreographs ECM remodeling and EMT in GBM via transcriptional regulation of HSPB1. Lumefantrine, an antimalarial drug, inhibits the transcriptional activities of Fli-1 and its downstream targets HSPB1, ECM remodeling, and EMT. Lumefantrine is selectively cytotoxic and promotes apoptosis in GBM and reverses radio/TMZ resistance in GBM. This drug can easily be repurposed for management of GBM. Identification of drugs like lumefantrine from FDA-approved therapeutic agents and uncommon sources provides opportunities to broaden the breadth and versatility of current therapeutic regimens for GBM.

Author contributions: Y.R., A.B., M.M., and P.B.F. designed research; Y.R. and A.B. performed research; Y.R., A.B., U.K., I.B., S.D., S.M., S.K.D., L.E., W.K.C., and P.B.F. analyzed data; and Y.R., S.K.D., L.E., W.K.C., and P.B.F. wrote the paper.

Reviewers: A.G., Temple University; and J.G., National Cancer Institute.

The authors declare no competing interest.

[1]To whom correspondence may be addressed. Email: wcavenee@ucsd.edu, mahitosh@smst.iitkgp.ac.in, or paul.fisher@vcuhealth.org.

This article contains supporting information online at https://www.pnas.org/lookup/suppl/doi:10.1073/pnas.1921531117/-/DCSupplemental.

First published May 14, 2020.

addition, molecular docking studies were performed to understand the interaction pattern of lumefantrine at the binding site of Fli-1, and this interaction was further confirmed by isothermal titration calorimetry (ITC). Toxicity profiling of lumefantrine on major organs, including liver, spleen, lungs, heart, and kidney, was also performed. Taken together, these studies provide compelling evidence that targeting Fli-1 using lumefantrine has potential as an effective therapy for treating both primary GBM and radio/TMZ-resistant GBM.

Results and Discussion

GBM accounts for the majority of brain tumors with a poor patient prognosis, despite current interventional therapeutic strategies (surgery, radiation, and/or chemotherapy) (1–5). In principle, defining promising GBM-specific therapeutic targets could serve as a basis for developing strategies to advance effective therapies for GBM by elucidating the molecular pathways involved in gliomagenesis (2–5). Heat shock proteins (HSPs) provide a primary protein signature for GBM progression serving as a nexus for ECM remodeling and EMT (6). We previously demonstrated that specific HSPs, particularly HSPB1, are up-regulated in GBM and radio/TMZ-resistant GBM (8). Accordingly, inhibiting the transcriptional regulation of HSPB1 is an appealing strategy for creating a therapeutic approach to selectively target therapy-resistant GBM cells. We reported a potentially relevant transcription factor, Fli-1, located in the 5-kb upstream region of the HSPB1 gene as an important mediator of HSPB1 expression (8). Fli-1 was shown to functionally regulate HSPB1 expression, and using an innovative drug screening strategy, a selective inhibitor of Fli-1 was identified.

Isolation of Fli-1 Inhibitors from Small-Molecule Libraries. Fli-1 and HSPB1 expression were evaluated by Western blot analysis in five GBM cell lines: U87MG, LN229, LN18, T98G, and A172 (Fig. 1 *A* and *B*). Based on these initial studies, we focused on U87MG and T98G cells. To identify small molecules capable of inhibiting Fli-1 transactivation ability, luciferase assays were performed using an engineered Fli-1 vector (Fli-1 Ets DNA-binding site cloned in front of a minimal promoter, upstream of a luciferase reporter gene), designated Fli-1-Lu (Fig. 1*C*). Exogenous expression of Fli-1 produces more robust luciferase activity compared with endogenous Fli-1 expression. Accordingly, an Fli-1 expression vector, murine stem cell virus (MSCV) neo-Fli-1, was used in screening for Fli-1 inhibitors. T98G cells were cotransfected with an Fli-1-Lu construct and an MSCV neo-Fli-1 vector (Fig. 1*C*). The negative controls were T98G cells cotransfected with Fli-1-Lu and MSCV empty vector to exclude drugs that could inhibit luciferase activity through an Fli-1–independent pathway.

Screening experiments were performed using biologically and pharmacologically active compounds, natural products and marketed drugs. In Ewing's sarcoma (EWS), a chromosomal translocation generating a fusion of the transactivation domain of EWS with the Ets domain of Fli-1 has been well documented (14). Thus, the drugs used for screening were selected on the basis of the structure-activity relationship from the EWS class of inhibitors, including naphthoquinones, monochlorobenzenes, nitrofuran, and benzamidines. Library screening identified 17 compounds that efficiently reduced Fli-1–mediated luciferase activity by 50% (*SI Appendix*, Table S1). The lead compounds were further screened by docking them with Fli-1 DNA-binding domains resulting in the selection of four compounds for further investigation.

Four lead compounds (furamidine, nifurtimox, lumefantrine, and atovaquone) were assayed for cytotoxicity in SVGp12 cells (normal astroglial cells). These four compounds showed minimal cytotoxicity with IC_{50} values of 289.7 μM for furamidine, 319.1 μM for nifurtimox, 732.2 μM for lumefantrine, and 450.9 μM for

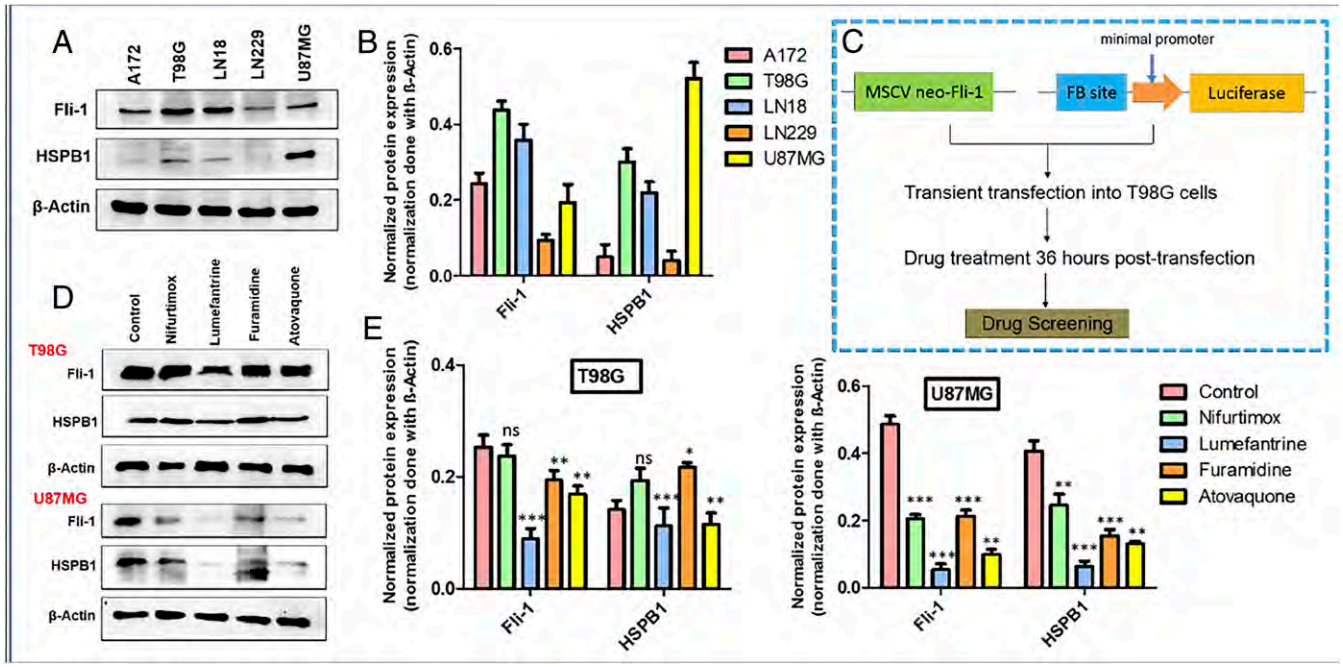

Fig. 1. Fli-1 drug screening. (*A* and *B*) Relative expression of Fli-1 and HSPB1 in five different GBM cell lines determined by Western blot analysis (*A*) and normalization of expression (based on β-actin expression) (*B*). (*C*) Schematic representation of the Fli-1 drug-screening strategy. Fli-1-Lu: multiple copies of the Fli-1 consensus-binding site (FB site) cloned upstream of a minimal promoter immediately upstream of the luciferase gene. MSCV neo-Fli-1: Fli-1 gene cloned into the MSCV vector. Luciferase gene driven by the Luc promoter: Fli-1-Lu was cotransfected with either MSCV neo-Fli-1 or MSCV empty vector into T98G cells. Cells were treated with various drugs at 36 h posttransfection and screened for efficient down-regulation of luciferase activity. (*D*) Relative expression by Western blot analysis of Fli-1 and HSPB1 in T98G and U87MG cells treated with positive inhibitory candidates identified using the Fli-1 drug screening protocol. (*E*) Corresponding densitometry plot for *D* showing normalization of expression (based on β-actin expression). Each bar represents average of three independent experiments. The level of significance is indicated as $*P < 0.05$, $**P < 0.01$, or $***P < 0.001$.

atovaquone (*SI Appendix*, Fig. S1*A*). These molecules displayed antiproliferative effects in U87MG and T98G cells (GBM cells). The IC_{50} values for furamidine, nifurtimox, lumefantrine, and atovaquone were 94.6 μM, 151.2 μM, 77.1 μM, and 50.7 μM, respectively, in U87MG cells and 128.1 μM, 101.2 μM, 37.4 μM, and 92.6 μM, respectively, in T98G cells (*SI Appendix*, Fig. S1 *B* and *C*). Among these four lead compounds, the Fli-1 inhibitor chosen for further studies was determined by evaluating the activity on Fli-1 and HSPB1 protein at a translational level. The T98G and U87MG cells were exposed to IC_{50} doses for 12 h and were lysed at 24 h after drug treatment, followed by Western blot analysis (Fig. 1 *D* and *E*). This approach identified lumefantrine as a potential therapeutic agent inhibiting Fli-1 transactivating activity. Lumefantrine is a Food and Drug Administration (FDA)-approved aryl-amino alcohol antimalarial drug used in combination with artemether to treat malaria (26).

Lumefantrine-Binding Affinity to the Fli-1 Protein. Phase-contrast microscopy images of lumefantrine-treated U87MG and T98G cells showed morphological changes suggestive of apoptotic cell death (*SI Appendix*, Fig. S2*A*, arrows). Lumefantrine inhibited wound healing, migration, infiltration, and anchorage-independent growth in U87MG and T98G cells (*SI Appendix*, Fig. S2 *B–D*). In addition, lumefantrine significantly reduced the enzymatic activity of MMP-2 and MMP-9 in U87MG and T98G cells (*SI Appendix*, Fig. S2*E*). A dose-dependent antiproliferative effect was also observed in lumefantrine-treated radio/TMZ-resistant cells (*SI Appendix*, Fig. S1 *D* and *E*). Half-maximal inhibitory concentration (IC_{50}) values of lumefantrine were 137.2 μM in U87MG RR cells, 73.1 μM in T98G RR cells, 185.3 μM in U87MG TMZR cells, and 120.2 μM in T98G TMZR cells.

A direct interaction between lumefantrine and Fli-1 was confirmed by docking of lumefantrine with the DNA-binding domain of the Fli-1 protein (Fig. 2 *A–C*) and ITC. The chemical structure of lumefantrine is shown in Fig. 2*B*. The ITC thermogram and fitted binding isotherm (Fig. 2*D*) displayed the following thermodynamic parameters of lumefantrine's binding to Fli-1 protein: ΔH (enthalpy), −1.349E4 ± 1,349 cal/mol; ΔS

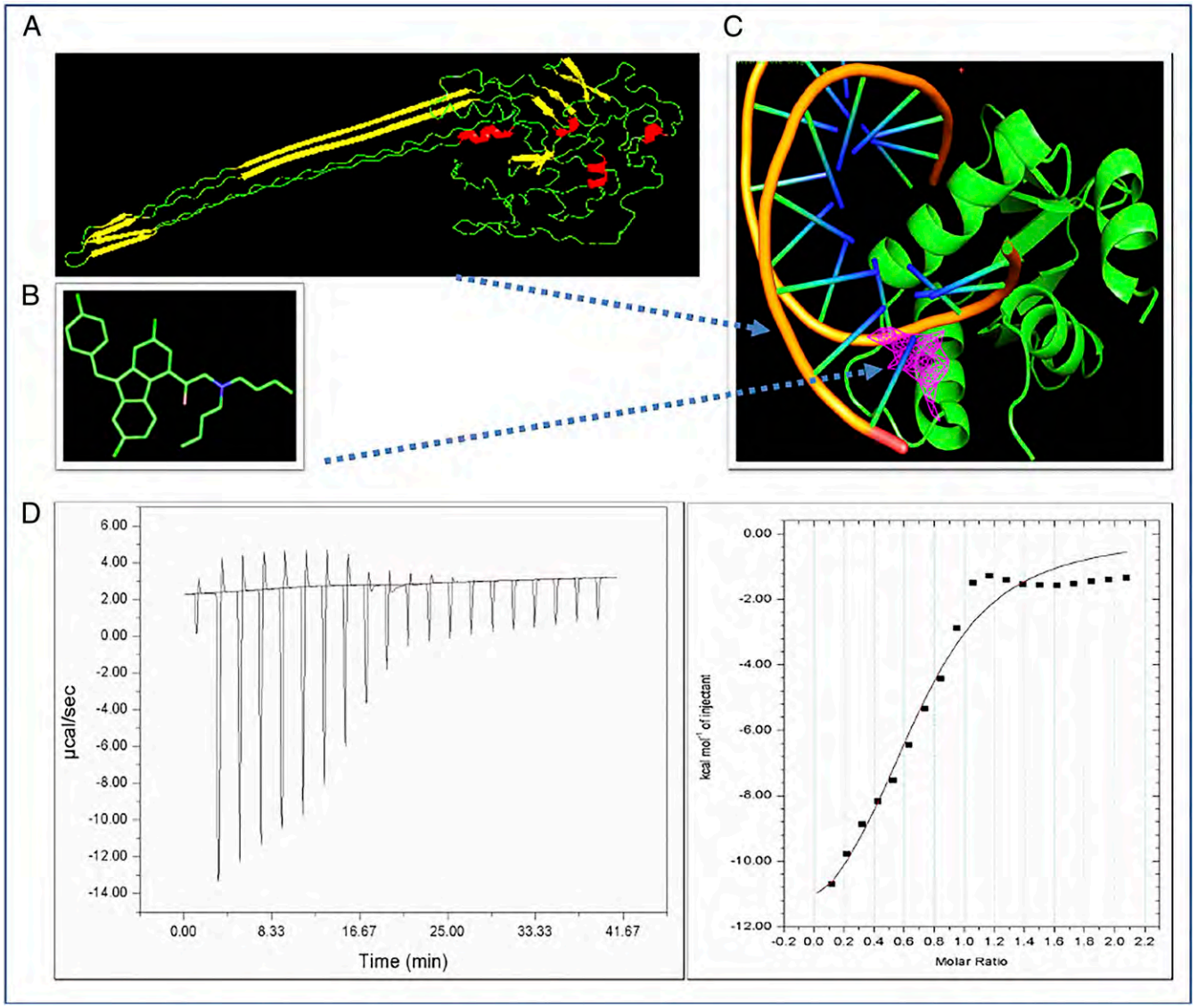

Fig. 2. Interaction between lumefantrine and Fli-1 protein. (*A*) The three-dimensional structure of Fli-1 protein using I-TASSER. (*B*) Chemical structure of lumefantrine. (*C*) Docked conformation of lumefantrine with the DNA-binding domain of Fli-1 protein. (*D*) ITC thermogram and fitted binding isotherm. Direct interaction between lumefantrine and Fli-1 was measured by ITC. The thermodynamic parameters of binding of lumefantrine to Fli-1 are as follows: ΔH (enthalpy), −1.349E4 ± 1,349 cal/mol; ΔS (entropy), −27.8 cal/mol/deg; K_d (dissociation constant), 6.5 μM; and N (stoichiometry), 0.687 ± 0.0496.

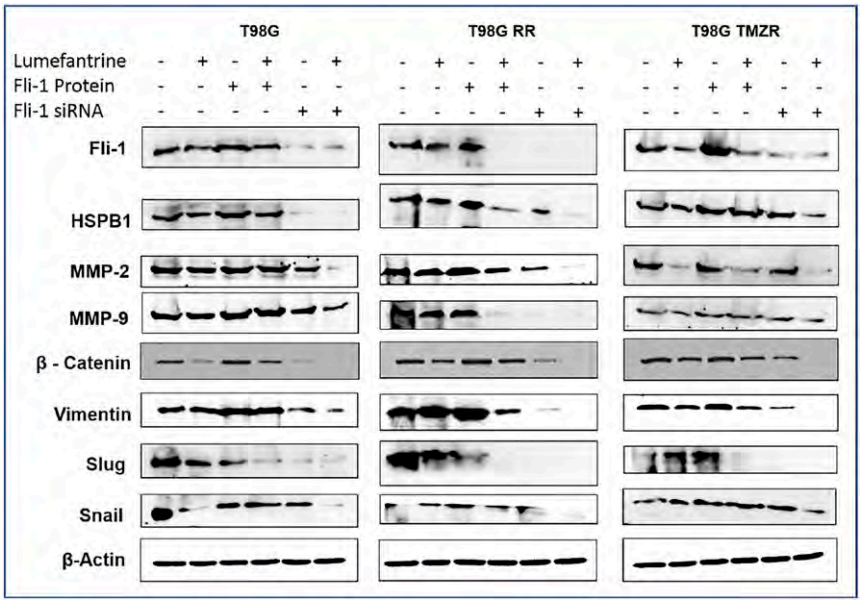

Fig. 3. Lumefantrine-mediated inhibition of Fli-1 for the treatment of radio/TMZ-resistant GBM. Lumefantrine inhibits Fli-1, HSPB1, MMP-2/-9, and EMT markers in Fli-1 protein and Fli-1 siRNA-treated T98G, T98G RR, and T98G TMZR cells. Densitometry plots are shown in *SI Appendix*, Fig. S3.

(entropy), −27.8 cal/mol/degree; K_d (dissociation constant), 6.5 μM; and N (stoichiometry), 0.687 ± 0.0496. These studies confirm that lumefantrine affects the in vitro properties of GBM and radio/TMZ-resistant GBM, and that it directly binds to the Fli-1 protein.

Lumefantrine Mediates Apoptosis and Inhibits Fli-1/HSPB1, MMP-2/-9, and EMT in Radio/TMZ-Resistant GBM Cells. To determine the effect of lumefantrine on GBM and GBM-resistant cells at a molecular level, T98G, T98G RR, and T98G TMZR cells were treated with Fli-1 protein for 3 h, transfected with Fli-1 siRNA and then treated with lumefantrine individually and in combination. Fli-1 siRNA, as well as lumefantrine treatment, robustly reduced expression of Fli-1, HSPB1, MMP-2, MMP-9, β-catenin, Vimentin, Slug, and Snail protein in all three cell lines (Fig. 3 and *SI Appendix*, Fig. S3). These results demonstrate comparable efficiencies of Fli-1 inhibitor and Fli-1 siRNA in terms of reduction of Fli-1 and HSPB1 protein expression. In addition, the inhibitor also significantly reduced Fli-1 and HSPB1 expression in the presence of Fli-1 protein.

Lumefantrine induced apoptosis in a time-dependent manner, as demonstrated by DNA content-based cell cycle analysis of

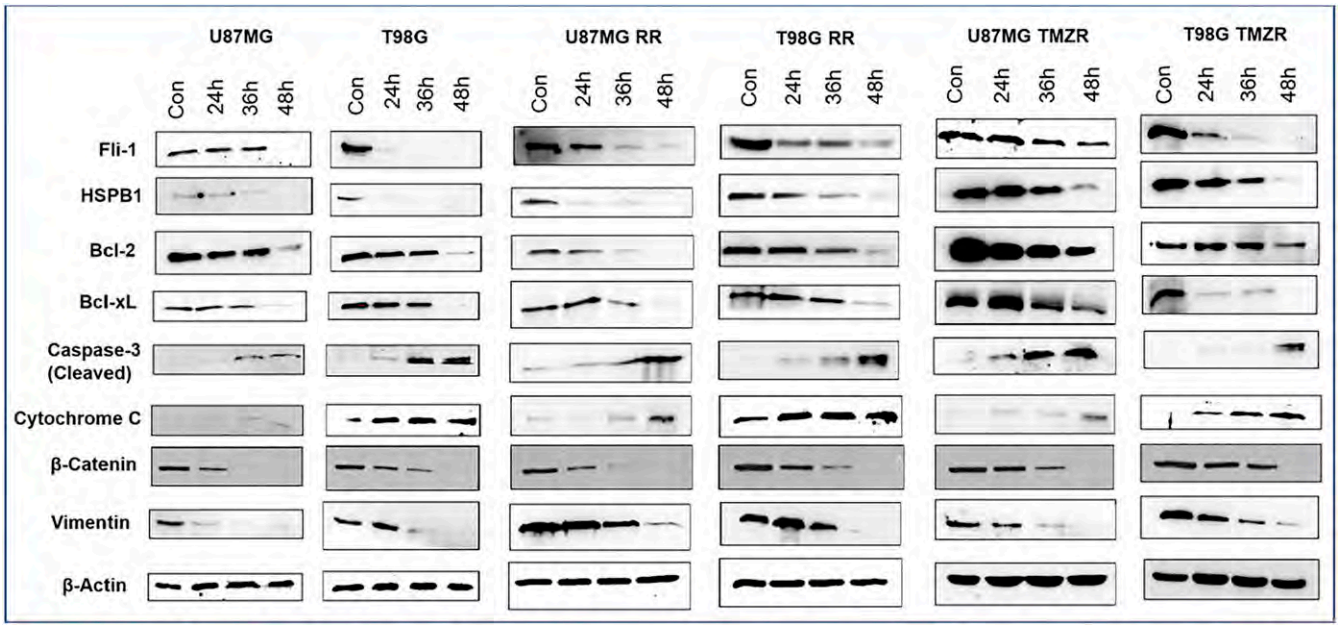

Fig. 4. Lumefantrine triggered apoptosis in GBM cells. Western blot analysis of Fli-1, HSPB1, EMT markers, and various proapoptotic and antiapoptotic proteins in U87MG, U87MG RR, U87MG TMZR, T98G, T98G RR, and T98G TMZR cells. GBM cells were grown and treated with lumefantrine (IC_{50} dose) for 24, 36, and 48 h. Expression of Bcl-2 and Bcl-xL were down-regulated, caspase activation was increased, and cytochrome *c* release was observed in lumefantrine-treated parental and resistant GBM cells. Densitometry plots are shown in *SI Appendix*, Fig. S6.

U87MG, U87MG RR, and U87MG TMZR cells (*SI Appendix*, Fig. S4*A*). Cells were grown in 60-mm tissue culture plates and treated with an IC_{50} dose of lumefantrine for 24, 36, and 48 h. The sub-G_1 population (apoptotic cells) was increased due to lumefantrine treatment (*SI Appendix*, Fig. S4*A*). Similar increases in the sub-G_1 population (apoptotic cells) were observed based on DNA content-based cell cycle analysis in T98G, T98G RR, and T98G TMZR cells exposed to lumefantrine (*SI Appendix*, Fig. S4*B*). To provide further confirmation that lumefantrine mediates apoptosis in parental and radio/TMZ-resistant GBM cells, annexin V/propidium iodide assays were performed in T98G, T98G RR, and T98G TMZR cells. As shown in *SI Appendix*, Fig. S5, lumefantrine caused a substantial increase in cell death by inducing apoptosis in all three cell lines, which was significantly reduced in the presence of a pan-caspase inhibitor Z-VAD (*SI Appendix*, Fig. S5).

Radio/TMZ-resistant GBM cells were grown and treated with lumefantrine (IC_{50} dose) for 12 h and after 24, 36, and 48 h, the cells were lysed and examined for molecular changes (Fig. 4 and *SI Appendix*, Fig. S6). In U87MG cells, Fli-1 and HSPB1 were down-regulated at 36 h, and in T98G cells, these genes were down-regulated at 24 h. In radiation-resistant cells, Fli-1 was down-regulated at 36 h and HSPB1 was vigorously down-regulated at 24 h in U87MG RR cells, while Fli-1 expression was extinguished at 48 h and HSPB1 expression was dramatically ablated at 36 h in T98G RR cells. In TMZ-resistant cells, Fli-1 and HSPB1 expression were significantly reduced at 48 h in U87MG TMZR cells, and Fli-1 expression was reduced at 24 h and HSPB1 expression was reduced at 48 h in T98G TMZR cells. These data provide solid evidence that lumefantrine is effective in suppressing Fli-1 and HSPB1 expression in radio/TMZ-resistant GBM after 24 h or 36 h of exposure, respectively. Expression of the antiapoptotic proteins Bcl-2 and Bcl-xL and EMT proteins β-catenin and vimentin were down-regulated in a time-dependent manner. Caspase activation and release of cytochrome *c* were evident in lumefantrine-treated GBM and radio/TMZ-resistant GBM cells.

Lumefantrine Inhibits Tumor Growth in U87MG, Radioresistant U87MG, and TMZ-Resistant U87MG Orthotopic Animal Models. Antitumor effects of lumefantrine were tested in U87MG radio/TMZ-resistant orthotopically injected animal models. A representative group of animals containing the various U87 GBM cell lines injected intracranially and either untreated or treated with lumefantrine were sacrificed at 2 and 4 wk. Tumor size and weight were lower at both time points in the lumefantrine-treated animals (*SI Appendix*, Fig. S7). After 28 d of treatment with lumefantrine (20 mg/kg for U87MG, 40 mg/kg for U87MG RR, and 50 mg/kg for U87MG TMZR), immunohistochemical analysis confirmed decreased expression levels of Fli-1 and HSPB1 in lumefantrine-treated U87MG and U87MG radio/TMZ-resistant animal models (Fig. 5*A*). Histopathological analyses of major organs, including brain, heart, lung, liver, spleen, and kidney, were performed after 28 d of treatment of U87MG, U87MG RR, and U87MG TMZR cells in mouse models. Hematoxylin and eosin (H&E) staining of organs from the different groups indicated no significant morphological changes following lumefantrine treatment in U87MG, U87MG RR, and U87MG TMZR animals. Only the organ toxicity H&E images for U87MG TMZR cells are provided, since these cells

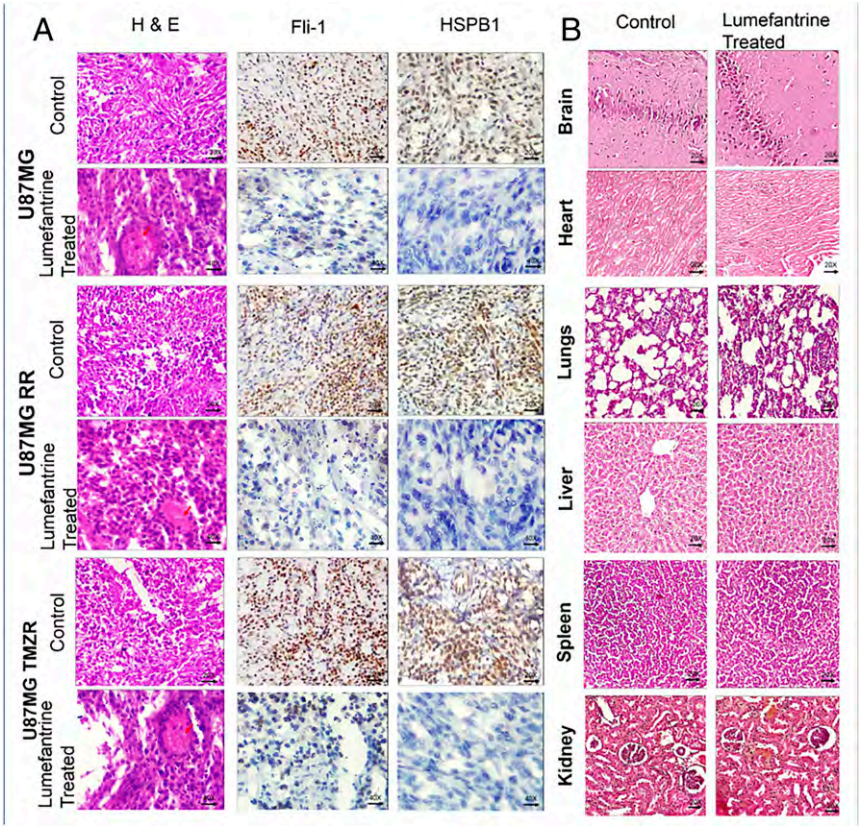

Fig. 5. Lumefantrine mediates inhibition of Fli-1 in vivo in U87MG, U87MG RR, and U87MG TMZR orthotopic GBM models. (*A*) Immunohistochemistry of tissue sections derived from different groups of orthotopic GBM models. Expression of Fli-1 and HSPB1 were significantly reduced in the treated groups. (*B*) H&E staining of major organs, including brain, heart, lungs, liver, spleen, and kidney, in the U87MG TMZR GBM model to detect any organ-specific toxicity induced by lumefantrine.

had received the highest dose of lumefantrine (50 mg/kg) among the three GBM models (Fig. 5*B*). The Fli-1 inhibitor displayed no toxic effects in these major organs. However, some toxic effects at this higher dose were found in liver and spleen based on morphological observations.

Protein expression in tissue lysates derived from tumors demonstrated that Fli-1, HSPB1, antiapoptotic protein Bcl-2, EMT markers, and ECM remodeling proteins were down-regulated, while the apoptotic protein Bax was up-regulated in the lumefantrine-treated groups (Fig. 6). These data support the in vitro observations and demonstrate antitumor effects and similar biochemical/molecular effects of lumefantrine on Fli-1/HSPB1/EMT markers/ECM remodeling protein networks in vivo in U87MG, U87MG RR, and U87MG TMZR mouse models.

In summary, the present study documents the importance and relevance of HSPB1 and Fli-1 in the regulation of radio/TMZ-resistance of GBM cells. They confirm that targeted inhibition of Fli-1/HSPB1–mediated EMT and ECM remodeling signaling axes by lumefantrine provides a novel therapeutic reagent for radio/TMZ resistance in glioblastoma (Fig. 7). These preclinical studies provide a solid rationale for Fli-1/HSPB1 inhibition with lumefantrine as a potentially selective approach for glioblastoma management. Although the safety profile of lumefantrine (an FDA-approved drug) is appropriate for clinical utility, further studies are needed to determine the efficiency of this new anti-glioblastoma drug to pass the blood-brain barrier (using an authentic primary intracranial GBM model) and also to evaluate additional combinatorial approaches for enhancing further therapeutic outcomes. Preliminary analysis using a computational blood-brain barrier algorithm (27) indicates that lumefantrine should pass through the blood-brain barrier (*SI Appendix*, Fig. S8). In addition, the screening strategy described in the paper using additional transcriptional targets and a diverse array of natural products, marketed drugs, and existing and new therapeutic agents offers potential for identifying additional drugs or drug combinations that may be of value in treating GBM, an aggressive and fatal cancer without any effective therapies (with recurrence at 7 mo after surgery; ref. 2). Further studies in other cancers in which Fli-1 expression is relevant would also be of value in defining additional applications of lumefantrine for potential cancer therapy.

Materials and Methods

Cell Cultures. The human GBM cell lines U87MG, A172, and LN18 were generously provided by Ellora Sen, National Brain Research Centre. LN229, T98G (human GBM), and SVGp12 cells (normal astroglial cells) were provided by Annapoorni Rangarajan, Indian Institute of Science. Cells were grown as described previously (7). Radio/TMZ-resistant GBM cell lines were selected as described previously (8). The GBM cell lines were authenticated by cell repository (National Centre for Cell Science).

Immunohistochemistry. Immunohistochemistry (IHC) analysis and hematoxylin and eosin (H&E) staining of orthotopic GBM tumors grown in nude mice were performed with different antibodies, including Fli-1 and HSPB1 (28), using a super-sensitive polymer-HRP (horseradish peroxidase) IHC detection system (QD420-YIKE; BioGenex). The secondary antibody poly-HRP reagent and peroxide-DAB (3,3′-diaminobenzidine) staining (for protein expression) provided in the kit was performed, followed by hematoxylin counterstaining for nuclear staining.

Wound Healing Assay. The migration potential of GBM cells was analyzed by wound-healing assays or scratch assays as described previously (29). The cells were seeded in a six-well plate, and a wound was drawn using a pipette tip on attaining ∼80% confluency. Washing in PBS (phosphate-buffered saline) was done to remove debris and suspended cells. The microscopic images were obtained at 0, 12 and 24 h under an inverted phase-contrast microscope (Leica Microsystems).

Boyden Chamber Assay. Boyden chamber assays were performed to check the invasive property of GBM cells as described previously (7). A total of 1×10^5 cells were suspended in serum-free medium and then added to the upper chamber. Chemoattractant (vascular endothelial growth factor and serum

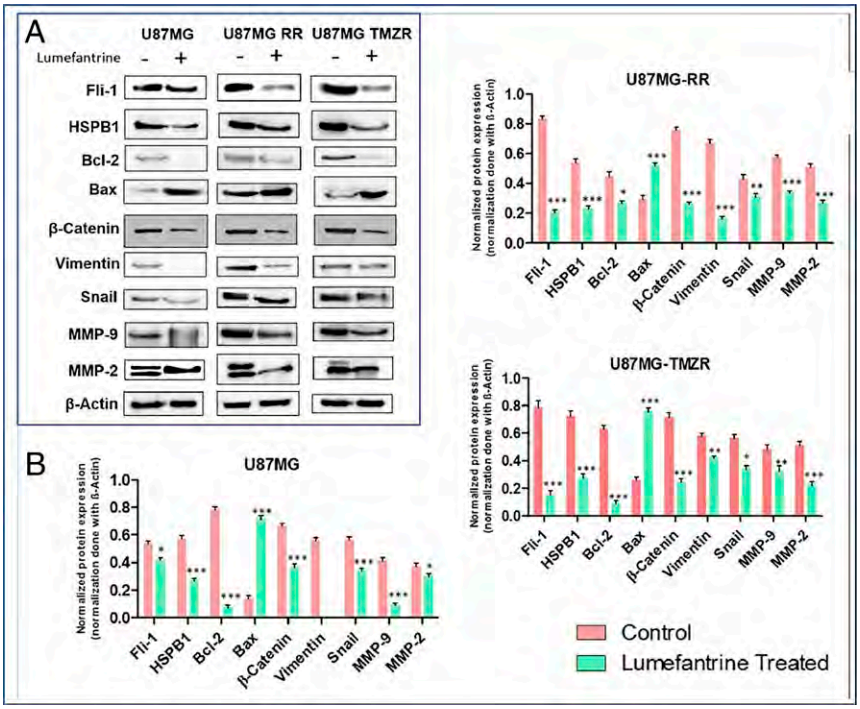

Fig. 6. Inhibition of Fli-1/HSPB1 axes by lumefantrine in an in vivo orthotopic GBM model. (*A* and *B*) Western blot analysis of tissue lysates derived from tumors confirming down-regulation of Fli-1, HSPB1, Bcl-2, β-catenin, Vimentin, Snail, MMP-9, and MMP-2 as well as up-regulation of Bax in lumefantrine-treated groups compared with controls. Each bar represents the average of three independent experiments. The level of significance is indicated by $*P < 0.05$, $**P < 0.01$, or $***P < 0.001$.

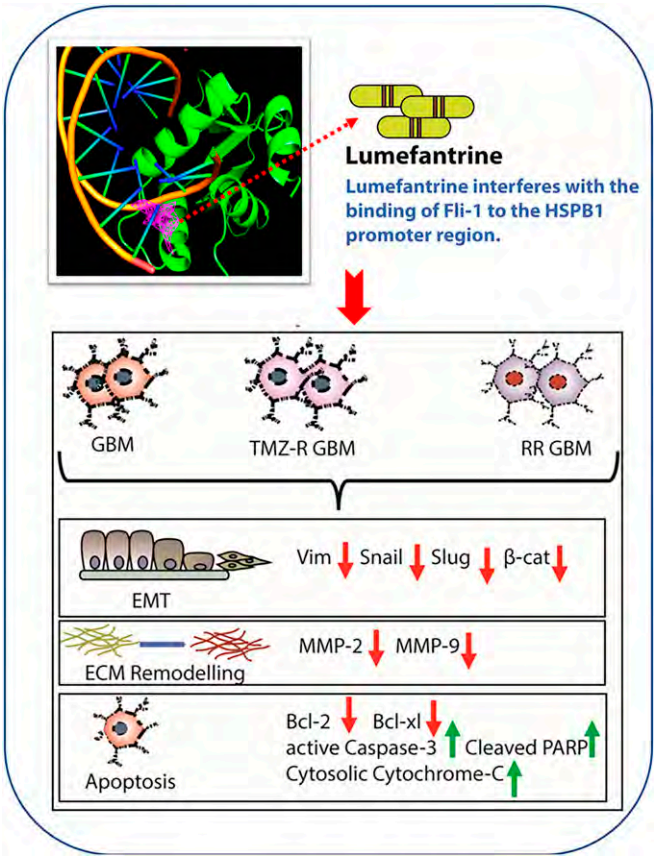

Fig. 7. Schematic outline of lumefantrine-mediated inhibition of Fli-1, a transcription factor in the upstream region of HSPB1, targeting radioresistance and TMZ resistance (RR/TMZR) in glioblastoma.

medium) was added in the lower compartment of the Boyden chamber, followed by incubation for 16 h at 37 °C. The nonmigrated cells were then removed by cotton swab, and migrated cells were fixed with 100% methanol. Bright-field images of migrated cells stained with H&E were obtained by microscopy.

Western Blot Analysis. Western blotting was performed to assess protein expression in human GBM and radio/TMZ-resistant cells as described previously (28). The cells were grown in six-well plates. After attaining 70% confluence, cells were treated with specific experimental reagents, harvested, and lysed with Nonidet P-40 lysis buffer (Invitrogen) according to the manufacturer's protocol after a stipulated treatment schedule. An equal amount of protein was separated by SDS/PAGE (sodium dodecyl sulfate/polyacrylamide gel electrophoresis), and separated proteins were transferred to a nitrocellulose membrane, followed by 3% BSA (bovine serum albumin) membrane blocking. Blocked membranes were washed and incubated with specific primary antibodies overnight at 4 °C. The membranes were then washed and exposed to specific secondary HRP-conjugated antibodies, followed by washing and developing in an ImageQuant LAS 4000 biomolecular imager (GE Healthcare).

Transfection Experiments. Transfection studies were performed to determine the effect of Fli-1 shRNA/siRNA on T98G/T98G RR/T98G TMZR cells. Cells were grown in Petri dishes and serum-starved overnight. The respective cells were transfected with Fli-1 shRNA/siRNA using a previously reported method (30). After 24 h of transfection, cells were lysed with Nonidet P-40 lysis buffer, and Western blot analysis was performed.

Cell Proliferation Assay. The antiproliferative effects of TMZ and lumefantrine on SVGp12, U87MG, T98G, U87MG RR, U87MG TMZR, T98G RR, and T98G TMZR cells were evaluated by MTT assays as described previously (31).

Binding Assay. To determine lumefantrine binding to the Fli-1 protein, we performed ITC using a MicroCal iTC200 system (GE Healthcare) as described previously (32). Initially, ITC was performed using a wide range of proteins (1 to 50 μM) in the instrument cell and 10× drug in the syringe. Recombinant human Fli-1 protein was obtained from Abcam and diluted to various concentrations with DNase/RNase-free water. The optimum binding curve was obtained at 20 μM Fli-1 protein and 180 μM lumefantrine. The cell and syringe in the calorimeter contained 2% DMSO (dimethyl sulfoxide). Titration was performed using 20 μM Fli-1 protein in sample cell and 180 μM lumefantrine in the injection. Experiments were performed at 25 °C as described previously (28).

Flow Cytometry Analysis. DNA content-based cell cycle analyses of lumefantrine-treated cells were performed by flow cytometry as described previously (32). In brief, U87MG, T98G, U87MG RR, U87MG TMZR, T98G RR, and T98G TMZR cells were seeded, grown and treated with an IC_{50} dose of lumefantrine. Treated cells were then processed and subjected to flow cytometry analysis.

In Vivo Orthotopic GBM Model. The antitumor effect of lumefantrine was assessed using U87MG cells in a nude mouse orthotopic model. The mice were housed at the Department of Biotechnology, Indian Institute of Technology in accordance with institutional guidelines. The experiments were approved by the Institutional Ethical Committee (project no. IE-6/MM-SMST/3.15) and were conducted observing all animal ethics regulations streamlined by the Institutional Animal Ethics Committee under guidance of the Indian government's Committee for the Purpose of Control and Supervision of Experiments on Animals.

A 5-μL Hamilton syringe fitted with a 26-gauge needle was used to inject 2.5 μL of complete culture medium containing 3×10^4 U87MG, U87MG RR, or U87MG TMZR cells as reported previously (28). After 12 d, tumors developed, and animals were divided at random into three main groups each with two subgroups (control and lumefantrine-treated): U87MG (control and treated with 20 mg/kg), U87MG RR (control and treated with 40 mg/kg), and U87MG TMZR (control and treated with 50 mg/kg). The treatment (via tail vein injection) regimens were followed with each group of six animals for 4 wk on alternate days. Western blot and immunohistochemistry analyses of tumor tissue and histopathology of major organs (brain, heart, liver, lungs, and spleen) were performed.

Statistical Analysis. Data are presented as mean ± SEM unless stated otherwise. Statistical significance was determined by two-way ANOVA followed by Student's *t* test.

Data Availability Statement. All data obtained for this study are presented in the main text and *SI Appendix*.

ACKNOWLEDGMENTS. Support for this work was provided by the Indian Department of Science and Technology's Innovation in Science Pursuit for Inspired Research (INSPIRE) Fellowship (IF130658), the Indian Institute of Technology Kharagpur and Ministry of Human Resource Development, the Indian Science and Engineering Research Board Fellowship (JCB/2019/000008), the Indian Council of Medical Research Grant (5/13/7/2019- NCD-III), the Indian Council of Scientific and Industrial Research Grant (27(0347)/19/EMR-II), and the Genetics Enhancement Fund of the Department of Human and Molecular Genetics and the VCU Institute of Molecular Medicine of VCU School of Medicine (S.K.D., L.E., and P.B.F.). P.B.F. is holder of the Thelma Newmeyer Corman Chair in Oncology at the VCU Massey Cancer Center.

1. Y. Rajesh *et al.*, Insights into molecular therapy of glioma: Current challenges and next-generation blueprint. *Acta Pharmacol. Sin.* **38**, 591–613 (2017).
2. S. K. Das, D. Sarkar, W. K. Cavenee, L. Emdad, P. B. Fisher, Rethinking glioblastoma therapy: MDA-9/Syntenin-targeted small molecule. *ACS Chem. Neurosci.* **10**, 1121–1123 (2019).
3. T. P. Kegelman *et al.*, MDA-9/syntenin is a key regulator of glioma pathogenesis. *Neuro-oncol.* **16**, 50–61 (2014).
4. T. P. Kegelman *et al.*, Inhibition of radiation-induced glioblastoma invasion by genetic and pharmacological targeting of MDA-9/Syntenin. *Proc. Natl. Acad. Sci. U.S.A.* **114**, 370–375 (2017).
5. S. K. Das, D. Sarkar, L. Emdad, P. B. Fisher, MDA-9/Syntenin: An emerging global molecular target regulating cancer invasion and metastasis. *Adv. Cancer Res.* **144**, 137–191 (2019).
6. Y. Rajesh, A. Biswas, M. Mandal, Glioma progression through the prism of heat shock protein-mediated extracellular matrix remodeling and epithelial to mesenchymal transition. *Exp. Cell Res.* **359**, 299–311 (2017).
7. Y. Rajesh *et al.*, Delineation of crosstalk between HSP27 and MMP-2/MMP-9: A synergistic therapeutic avenue for glioblastoma management. *Biochim. Biophys. Acta Gen. Subj.* **1863**, 1196–1209 (2019).
8. Y. Rajesh *et al.*, Transcriptional regulation of HSPB1 by Friend Leukemia Integration-1 factor modulates radiation and temozolomide resistance in glioblastoma. *Oncotarget* **11**, 1097–1108 (2020).
9. C. Yang, C. S. Hong, Z. Zhuang, Hypoxia and glioblastoma therapy. *Aging (Albany NY)* **7**, 523–524 (2015).

10. A. Hammerer-Lercher *et al*., Hypoxia induces heat shock protein expression in human coronary artery bypass grafts. *Cardiovasc. Res.* **50**, 115–124 (2001).
11. N. Qiao *et al*., Ets-1 as an early response gene against hypoxia-induced apoptosis in pancreatic β-cells. *Cell Death Dis.* **6**, e1650 (2015).
12. C. S. Foster *et al*., Hsp-27 expression at diagnosis predicts poor clinical outcome in prostate cancer independent of ETS-gene rearrangement. *Br. J. Cancer* **101**, 1137–1144 (2009).
13. I. G. Maroulakou, D. B. Bowe, Expression and function of ets transcription factors in mammalian development: A regulatory network. *Oncogene* **19**, 6432–6442 (2000).
14. T. Oikawa, T. Yamada, Molecular biology of the Ets family of transcription factors. *Gene* **303**, 11–34 (2003).
15. B. Davidson *et al*., Ets-1 messenger RNA expression is a novel marker of poor survival in ovarian carcinoma. *Clin. Cancer Res.* **7**, 551–557 (2001).
16. T. Oikawa, ETS transcription factors: Possible targets for cancer therapy. *Cancer Sci.* **95**, 626–633 (2004).
17. Y. Ben-David, E. B. Giddens, K. Letwin, A. Bernstein, Erythroleukemia induction by Friend murine leukemia virus: Insertional activation of a new member of the ets gene family, Fli-1, closely linked to c-ets-1. *Genes Dev.* **5**, 908–918 (1991).
18. Y. Ben-David, A. Bernstein, Friend virus-induced erythroleukemia and the multistage nature of cancer. *Cell* **66**, 831–834 (1991).
19. F. Liu, M. Walmsley, A. Rodaway, R. Patient, Fli1 acts at the top of the transcriptional network driving blood and endothelial development. *Curr. Biol.* **18**, 1234–1240 (2008).
20. D. D. Spyropoulos *et al*., Hemorrhage, impaired hematopoiesis, and lethality in mouse embryos carrying a targeted disruption of the Fli1 transcription factor. *Mol. Cell Biol.* **20**, 5643–5652 (2000).
21. E. E. Torlakovic *et al*., Fli-1 expression in malignant melanoma. *Histol. Histopathol.* **23**, 1309–1314 (2008).
22. W. Song *et al*., Oncogenic Fli-1 is a potential prognostic marker for the progression of epithelial ovarian cancer. *BMC Cancer* **14**, 424 (2014).
23. W. Song *et al*., Overexpression of Fli-1 is associated with adverse prognosis of endometrial cancer. *Cancer Invest.* **33**, 469–475 (2015).
24. M. N. Scheiber *et al*., FLI1 expression is correlated with breast cancer cellular growth, migration, and invasion and altered gene expression. *Neoplasia* **16**, 801–813 (2014).
25. X. Liang *et al*., Friend leukemia virus integration 1 expression has prognostic significance in nasopharyngeal carcinoma. *Transl. Oncol.* **7**, 493–502 (2014).
26. P. Byakika-Kibwika *et al*., Artemether-lumefantrine combination therapy for treatment of uncomplicated malaria: The potential for complex interactions with antiretroviral drugs in HIV-infected individuals. *Malar. Res. Treat.* **2011**, 703730 (2011).
27. H. Liu *et al*., AlzPlatform: An Alzheimer's disease domain-specific chemogenomics knowledgebase for polypharmacology and target identification research. *J. Chem. Inf. Model.* **54**, 1050–1060 (2014).
28. Y. Rajesh *et al*., Targeting NFE2L2, a transcription factor upstream of MMP-2: A potential therapeutic strategy for temozolomide-resistant glioblastoma. *Biochem. Pharmacol.* **164**, 1–16 (2019).
29. G. Dey *et al*., Therapeutic implication of "Iturin A" for targeting MD-2/TLR4 complex to overcome angiogenesis and invasion. *Cell. Signal.* **35**, 24–36 (2017).
30. G. Dey *et al*., Marine lipopeptide Iturin A inhibits Akt-mediated GSK3β and FoxO3a signaling and triggers apoptosis in breast cancer. *Sci. Rep.* **5**, 10316–14 (2015).
31. S. Parida *et al*., Gold nanorod embedded reduction responsive block copolymer micelle-triggered drug delivery combined with photothermal ablation for targeted cancer therapy. *Biochim. Biophys. Acta Gen. Subj.* **1861**, 3039–3052 (2017).
32. R. Bharti *et al*., Diacerein-mediated inhibition of IL-6/IL-6R signaling induces apoptotic effects on breast cancer. *Oncogene* **35**, 3965–3975 (2015).